C00-4030-4

# LASER DISCHARGES IN ATTACHING GASES

Final Report

for Period June 25, 1976 - June 24, 1977

G. L. Rogoff, L. E. Kline, J. L. Pack, and W. H. Kasner

Westinghouse R&D Center
Pittsburgh, Pennsylvania 15235



September 1977

Prepared For

THE U.S. ENERGY RESEARCH AND DEVELOPMENT ADMINISTRATION

UNDER CONTRACT NO. EY-76-C-02-4030

## DISCLAIMER

ABSTRACT

A significant problem in the development of high-power gas discharge lasers is the glow-to-arc transition, which limits the electrical energy that can be deposited in the diffuse glow plasma, especially in attaching gases. This report describes a combined experimental and theoretical study of the maintenance and stability of glow discharges in attaching gas mixtures similar to those used in rare gas-halide excimer laser discharges. A discharge test apparatus has been constructed for establishing uv-preionized, self-sustained, diffuse glow discharges in halogen-containing mixtures. Quasi-steady, diffuse discharges have been established in 0.5% $SF_6$:5-15% Kr:He mixtures at 100-800 Torr, and have been maintained for up to 1 μsec, the limit of the pulse-forming network used. Measured electric fields in the positive column agree well with fields calculated from a steady-state model based on electron production by one- and two-step electron impact ionization and loss by attachment to $SF_6$. The discharge duration is limited above some values of pressure, Kr concentration, and/or current density by the glow-to-arc transition, i.e., by filament formation within the diffuse glow. Discharge operation is not limited by the instability analyzed by Daugherty, Mangano, and Jacob.

TABLE OF CONTENTS

# I. INTRODUCTION

The glow-to-arc transition is an important limiting factor in the operation of many high-power gas discharge lasers, which require a diffuse glow plasma for proper performance; laser action terminates and system damage can occur when filamentary sparks develop within the plasma. Different types of discharges have been found to behave similarly during the glow-to-arc transition. Luminous filaments ($\sim$0.1 to 1 mm diameter) extend through the diffuse glow plasma from either one or both of the electrode regions. After a filament forms a channel completely across the discharge gap, an arc develops[1,2] to replace the diffuse glow. Similar phenomena appear, for example, in pulsed[3] and continuous[4] self-sustained high-power laser discharges and in electron-beam controlled devices,[5] as well as in low-overvoltage spark discharges,[1,2,6] which might seem to be substantially different than the laser discharges. Thus, the formation of filaments leading to arcs appears to be a general property of different types of discharges, with similar filament characteristics occurring in a variety of discharges.

An apparently general characteristic of discharges in attaching gases is that instabilities similar to those in nonattaching gases occur at lower pressures ($\sim$10-100 times lower[7]) and lower power inputs. Thus, the glow-to-arc instability appears to pose a particularly severe problem for the development of practical laser discharges in high-pressure mixtures that contain attaching gases.

Considerable effort has been applied to finding ways of avoiding arc formation in particular laser discharge devices. Most of this effort has consisted of empirical determination of the threshold for arc formation as a function of various system parameters. Although the results have proved useful for extending the operating range of particular systems and have provided ideas for techniques to be tried on new systems, relatively little has been learned about the instability mechanisms. An

understanding of the mechanism of filament formation[8,9] is essential to the development of a more generalized basis for avoiding arc formation.

A major impediment to significant progress has been the lack of detailed experimental data on the filament formation in laser discharges. This situation is to be contrasted with the situation for spark discharges, for which temporally and spatially resolved diagnostics have been performed. A real need exists for similar measurements on developing filaments in laser gas mixtures, especially in view of the interest in attaching-gas mixtures with the anticipated severity and importance of this problem for those cases. The present study is one step in an effort to understand the physics of filament formation in electronegative gas mixtures.

This report describes a combined experimental and theoretical study of the maintenance and stability characteristics of glow discharges in attaching gas mixtures involving processes similar to those in laser discharges, e.g., KrF. The emphasis of this study is on developing an understanding of discharge operation to serve as a foundation for examining the initial development of filaments during the glow-to-arc instability. Primarily, we have examined properties of the quasi-steady, diffuse glow discharge preceding the transition. A small-scale, flexible experimental discharge facility has been designed and fabricated to provide uv-preionized, self-sustained discharges in selected, representative gas mixtures, with the dominant discharge processes similar to those in laser discharges of interest. A pulse-forming-network power supply provides a steady discharge voltage for quasi-steady operation. This report describes the operation of quasi-cw, diffuse discharges in $He/Kr/SF_6$ gas mixtures. The mixtures are similar to those used in excimer laser systems.[10] Also, since considerable basic data are available for these components and they are relatively well-behaved experimentally, the mixtures provide good representative discharges for studies of general discharge characteristics.

## II. THEORY

### A. Quasi-Steady Discharge

A theoretical model has been developed to describe self-sustained discharge operation in gas mixtures at high pressure. This model predicts the electric field in the positive column of a high pressure discharge as a function of the discharge current density. The calculation proceeds in three steps:

1) First, the Boltzmann (i.e., electron energy balance) equation is used to check the consistency between available measured, calculated or estimated electron-heavy particle collision cross sections and measured electron transport parameters. This step is carried out for each individual gas species of interest. The method used is described by Frost and Phelps.[11] Details of the numerical techniques and the computer code are given by Luft.[12]
2) Next, the sets of cross sections determined in step (1) are used to calculate electron impact excitation and ionization rates for mixtures of gases. The Boltzmann equation is also solved in this second step of the analysis.
3) Finally, a set of rate equations is solved to calculate the steady state and time dependent densities of charged, excited, and neutral species in the discharge. The rate equation solution uses the electron-heavy particle collision rates determined in step (2) and heavy particle-heavy particle collision rates from the literature. The discharge current density is also calculated.

The first step has been carried out in order to determine sets of cross sections for Kr and $SF_6$. These Kr and $SF_6$ cross sections were then used, together with previously published cross sections[13] for He and excited Kr atoms[14] (Kr*) to calculate electron-heavy particle collision

rates for three He:Kr:$SF_6$ mixtures with the mixture proportions He:Kr:$SF_6$ = 94.5:5:0.5, 89.5:10:0.5, and 84.5:15:0.5. The proportions are expressed as percentages. The Kr* is included in the calculations in order to account for further excitation and ionization of excited atoms. The excited atom density, n*, is given relative to the total gas density, N. Finally, a rate equation model was used to calculate the steady state electric field in the positive column of a glow discharge as a function of the discharge current density. This calculation was carried out for all three mixtures. Several time dependent discharge calculations were also performed.

Electron Impact Cross Sections for Krypton

When this study began, a consistent set of electron impact collision cross sections for krypton was not available. The published analysis of Frost and Phelps[15] does give a momentum transfer cross section which is consistent with measured electron drift velocities. An electron impact ionization cross section is also available from the experimental work of Rapp and Englander-Golden.[16] A total cross section for electronic excitation was determined by combining the excitation cross section of Schapner and Schreiber[17] for electron energies $\varepsilon < 14$ eV and the total excitation cross section of Kuripanov[18] for $\varepsilon > 14$ eV. The Kuripanov cross section was normalized to have the same value ($3 \times 10^{-17}$ cm$^2$) as the Schapner and Schreibner cross section at 14 eV. This cross section was then adjusted in magnitude by comparing theoretical values of $\alpha$, the Townsend ionization coefficient, with values measured by Kruithof.[19] The theoretical values of $\alpha$ are obtained by solving the Boltzmann equation. The theoretical and experimental values of $\alpha$ agreed well when the measured cross section was multiplied by 1.2. The resulting total electronic cross section for krypton is given in Table I. The theoretical and experimental values of $\alpha$ are compared in Fig. 1. The data are given in the units of the experimental data, $\alpha/p_o$ vs. $E/p_o$, where $p_o = 273 \times p$ (Torr)/T(°K) is the gas pressure referred to 273°K, and E is the electric field.

A similar analysis has been carried out for kyrpton by Jacob and Mangano.[20] They concluded that the Schapner and Schreibner cross

Table I. Total cross section for electronic excitation of krypton by electron impact.

| Energy eV | Cross Section $10^{-16}$ $cm^2$ | Energy eV | Cross Section $10^{-16}$ $cm^2$ |
|---|---|---|---|
| .0 | .0000 | 13 | .20 |
| 9.9 | .0000 | 14 | .30 |
| 10.0 | .0125 | 20 | 1.45 |
| 10.3 | .0450 | 30 | 1.45 |
| 10.7 | .0350 | 40 | 1.00 |
| 11.0 | .0650 | 80 | .90 |
| 12.0 | .1300 | 140 | .45 |

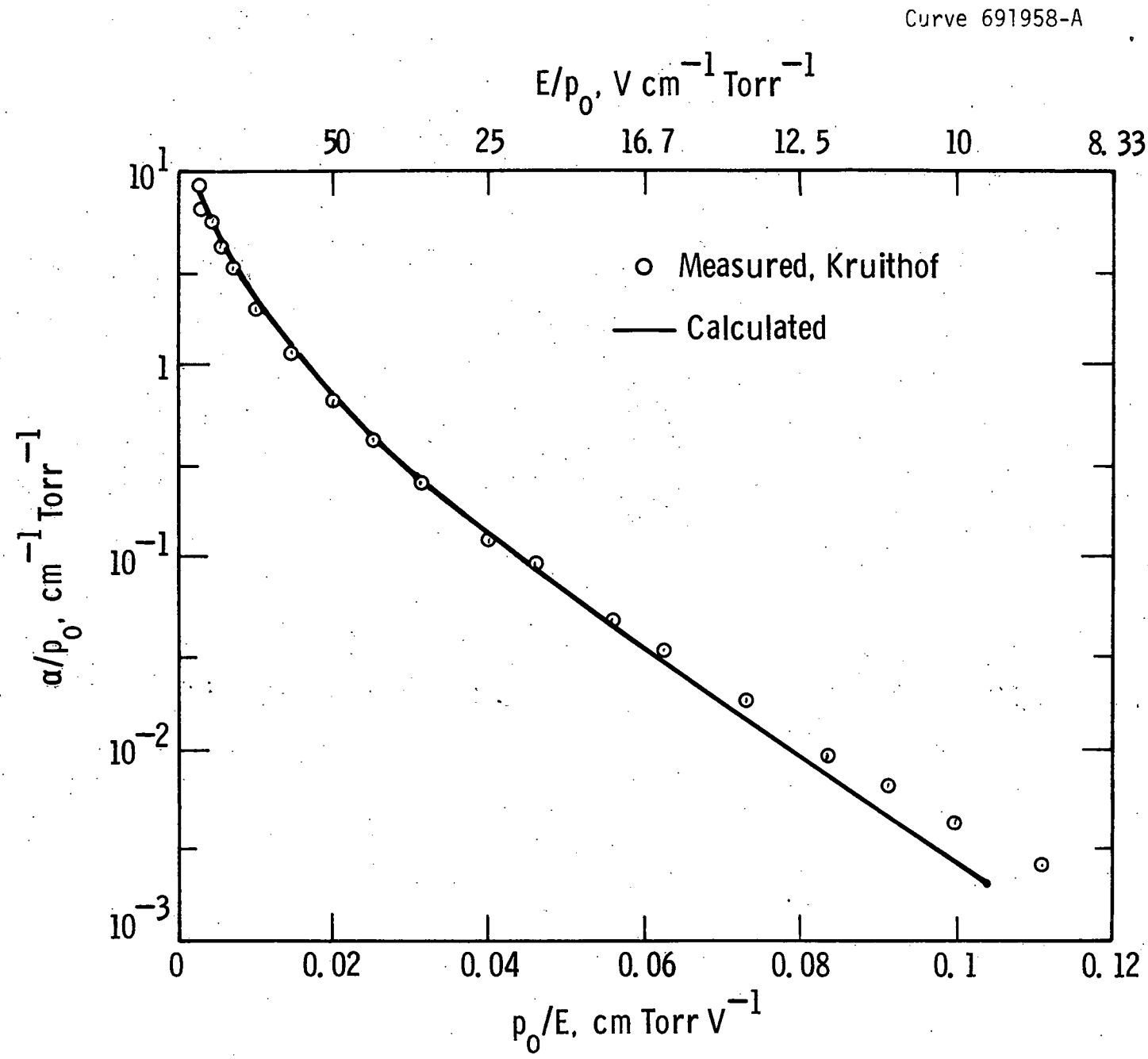


Fig. 1. Measured and calculated values of the Townsend ionization coefficient, $\alpha/p_o$, vs. $p_o/E$ for krypton.

sections should be multiplied by 0.97 to obtain agreement between measured and calculated values of $\alpha$. However, their conclusion is based on a comparison at small values of E/p where $\alpha$ is small and difficult to measure. The present analysis considers a much wider range of E/p and emphasizes the range E/p > 15 Volts/cm Torr, where $\alpha$ is larger and can be more accurately measured. Consequently, the cross section determined in our analysis is believed to be more reliable than the cross section given in Ref. 20.

Electron Impact Cross Sections for Sulfur Hexafluoride

Electron swarm data for $SF_6$ have been obtained by a number of experimenters, primarily because of interest in $SF_6$ as a dielectric gas. However, cross section data has been very limited until recently, and we are not aware of any previous Boltzmann analyses for $SF_6$.

In our analysis we have used the recent momentum transfer cross section measurements of Srivastava et al[21] along with the unpublished attachment cross sections of Chen and Chantry[22] and the ionization cross section of Ref. 16. The four largest cross sections measured by Chantry and Chen, in order of peak cross section, lead to the formation of $SF_6^-$, $SF_5^-$, $F^-$, and $SF_4^-$. The cross sections for the formation of $SF_6^-$ and $SF_5^-$ are similar to those of Christophorou et al[23] while those for the formation of $F^-$ and $SF_4^-$ are similar to the cross sections of Lehmann.[24] Unfortunately, almost no data were available on the cross sections for vibrational or electronic excitation of $SF_6$ when the present analysis was carried out. However, we were able to determine an electronic cross section which gives good agreement between measured and calculated values of $\alpha$ and of the attachment coefficient, $\eta$. The measured[25-28] and calculated values of $\alpha$ and $\eta$ are compared in Fig. 2. These data are referred to $p_{20}$ = 293 x p (Torr)/T(°K). The total cross section for electronic excitation that we have determined is given in Table II. The Boltzmann analysis also predicts values of the electron drift velocity, W, and the electron characteristic energy, $D/\mu$. The characteristic energy is an experimentally accessible measure of the electron mean energy where $\mu \equiv W/E$ is the electron mobility and D is the electron diffusion coefficient in the direction normal to the applied electric field. The

Curve 691959-A

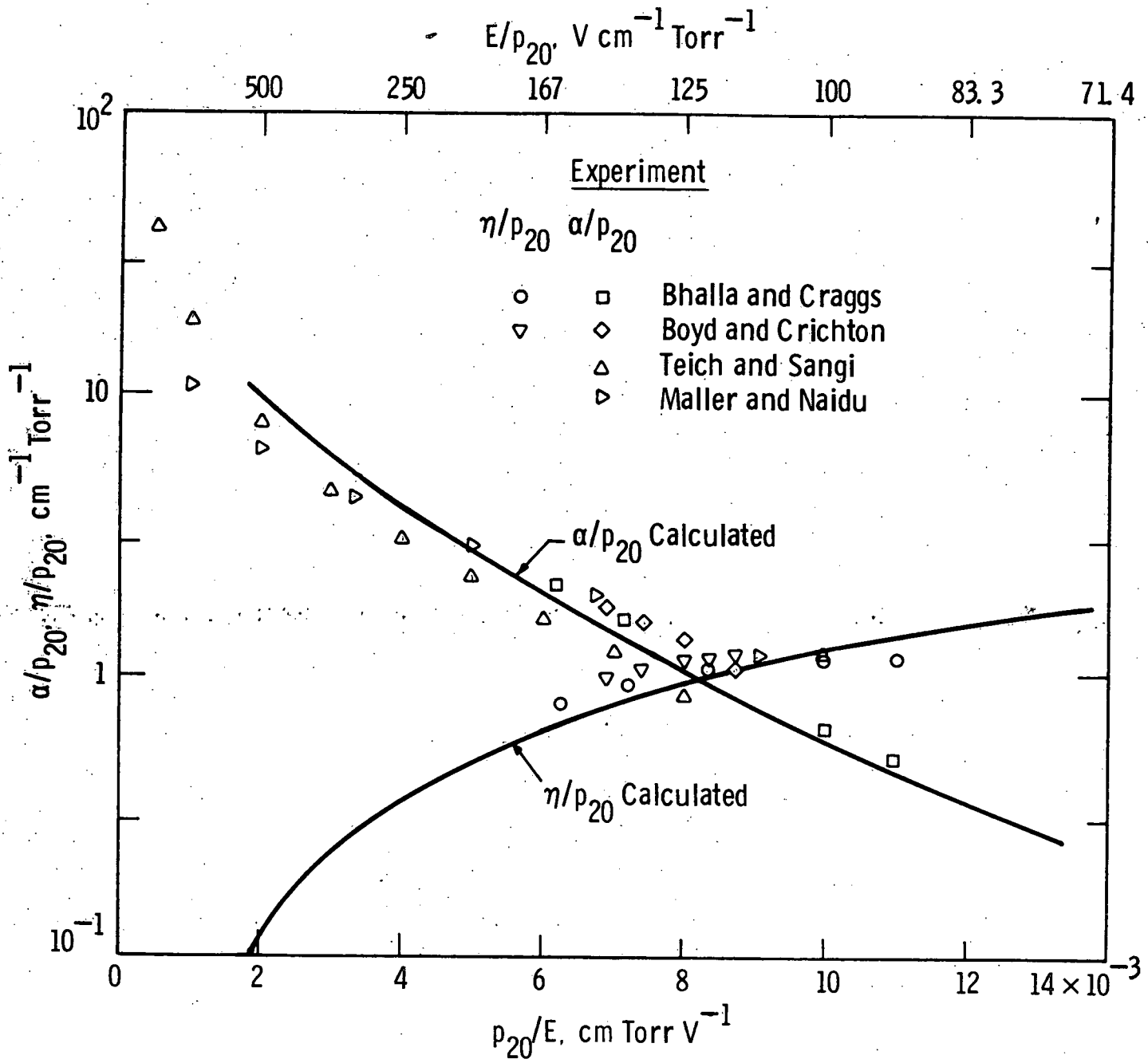


Fig. 2. Measured and calculated values of the Townsend ionization coefficient $\alpha/p_{20}$ and the attachment coefficient $\eta/p_{20}$ vs $p_{20}/E$ for $SF_6$.

Table II. Total cross section for electronic excitation of $SF_6$ by electron impact.

| Energy eV | Cross Section $10^{-16}$ $cm^2$ |
|---|---|
| 0 | 0 |
| 10 | 0 |
| 30 | 4 |
| 50 | 20 |
| 150 | 40 |

predicted values of W and $D/\mu$ are in fair agreement with those measured by Naidu and Prasad[29] with a maximum disagreement of about 30% for both transport coefficients.

Electron Energy Balance Calculations for $He:Kr:SF_6:Kr^*$ Mixtures

We have calculated the various electron impact excitation and ionization coefficients and the electron drift velocity in $He:Kr:SF_6:Kr^*$ mixtures. The excited krypton atoms are represented in the calculations by the excitation and ionization cross sections of Jacob and Mangano.[14] The other cross sections used as input data are the Kr and $SF_6$ cross sections described above and the He cross sections of Ref. 13.

The rate coefficients are calculated by numerically solving the Boltzmann or electron energy balance equation. In the calculations we have neglected electron-electron (e-e) and electron-ion (e-i) collisions. Recently published results[30] indicate that e-e and e-i collisions are important at high current densities when argon is the major constituent of the gas mixture. However, additional unpublished work[31] indicates that e-e and e-i collisions are unimportant when helium is the major constituent. We have also neglected superelastic collisions between excited atoms and electrons. Recent unpublished calculations[32] indicate that superelastic collisions are unimportant except at high current densities, beyond the range of the experimental measurements in the present study.

When electron-electron, electron-ion, and superelastic collisions are neglected, the independent parameters which specify a unique solution of the Boltzmann or electron energy balance equation are the mixture proportions, including the fractional density of excited atoms, and the electric field-to-total gas density ratio, E/N.

The excited atoms are potentially important not only because they can be easily ionized (two-step ionization) but also because the assumed thresholds for excitation (1.6 eV) and ionization (4.1 eV) of $Kr^*$ are much lower in energy than any other inelastic process except attachment to $SF_6$ and have large cross sections.[14] Thus the energy loss in excitation and ionization of $Kr^*$ can significantly affect the electron energy balance and the calculated rate coefficients even when the

fractional excited atom density, $n^*/N$, is small. We have examined the variation, as a function of $n^*/N$, of the coefficients for attachment to $SF_6$, $\alpha_a/N$, ionization of Kr*, $\alpha_2/N$, excitation of Kr, $\alpha_*/N$, and ionization of all species, $\alpha/N$. (The units are (collisions/cm) $cm^3$ = $cm^2$.) The calculation was performed for a $He:Kr:SF_6$ = 94.5:5:0.5 mixture with E/N = 16.95 Td. The units of E/N are Townsends (Td) where 1 Td $\equiv 10^{-17}$ V $cm^2$. The results of this calculation are shown in Fig. 3. When $0 < n^*/N < 6 \times 10^{-5}$ all four coefficients vary by less than 20% and the effect of the excited krypton on the calculated values of these coefficients, and on the electron energy balance, can be neglected. The predicted value of $n^*/N$ is less than $6 \times 10^{-5}$ for current densities less than 10 A/$cm^2$.

The calculated electron energy distribution in a $He:Kr:SF_6$ = 94.5:5:0.5 mixture is shown in Fig. 4 for the case where E/N = 18.8 Td and $n^*/N = 10^{-5}$. Calculated energy distributions for pure helium and pure krypton at the same value of E/N are also shown in the figure. Note that the electron energy distribution in the mixture is about midway between the helium and krypton energy distributions even though the mixture contains only 5% krypton. The results of the electron energy balance calculations in this mixture with E/N = 17 Td, a value representative of discharge operation, show that 66% of the input electrical energy goes to excitation and ionization of krypton. The other significant loss channels are elastic collisions (23%) and excitation of $SF_6$ (10%). All other losses, including excitation and ionization of helium, are negligible. An energy balance calculation for discharge operating conditions in the 15% Kr mixture shows that 81% of the input electrical energy goes to excitation and ionization of krypton. The energy losses to elastic collisions and excitation of $SF_6$ decrease, respectively, to 14% and 5%. Other losses are again negligible.

The results of the electron energy balance calculations show that the Kr* excitation coefficient, $\alpha_*/N$, and the total ionization coefficient, $\alpha/N$, can be fitted by functions of the form

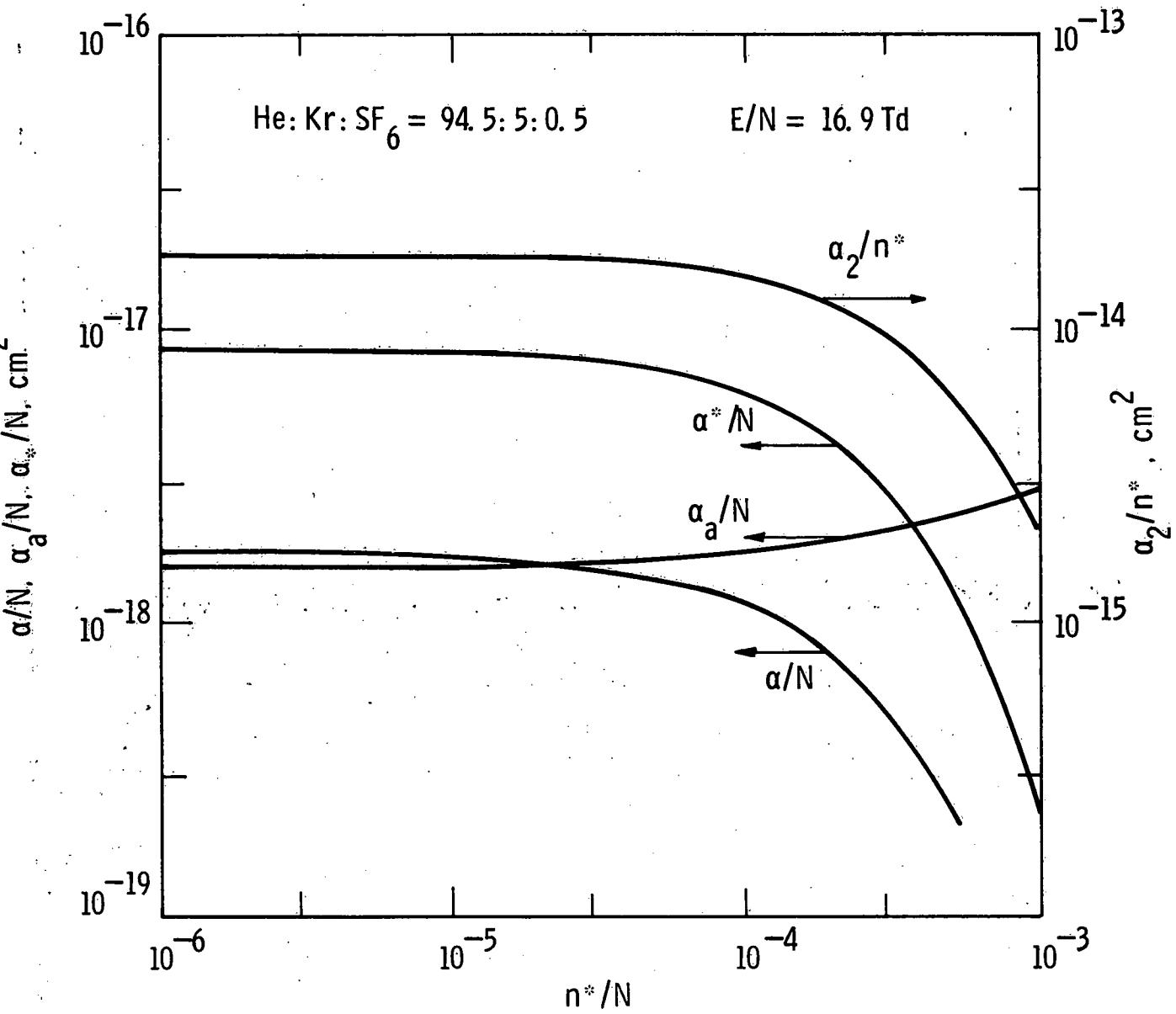


Fig. 3. Calculated electron-impact coefficients for total ionization of all species, ionization of excited krypton, attachment to $SF_6$, and excitation of krypton. The coefficients are plotted vs. the fractional density of excited krypton atoms. The gas mixture and the value of E/N are given in the figure.

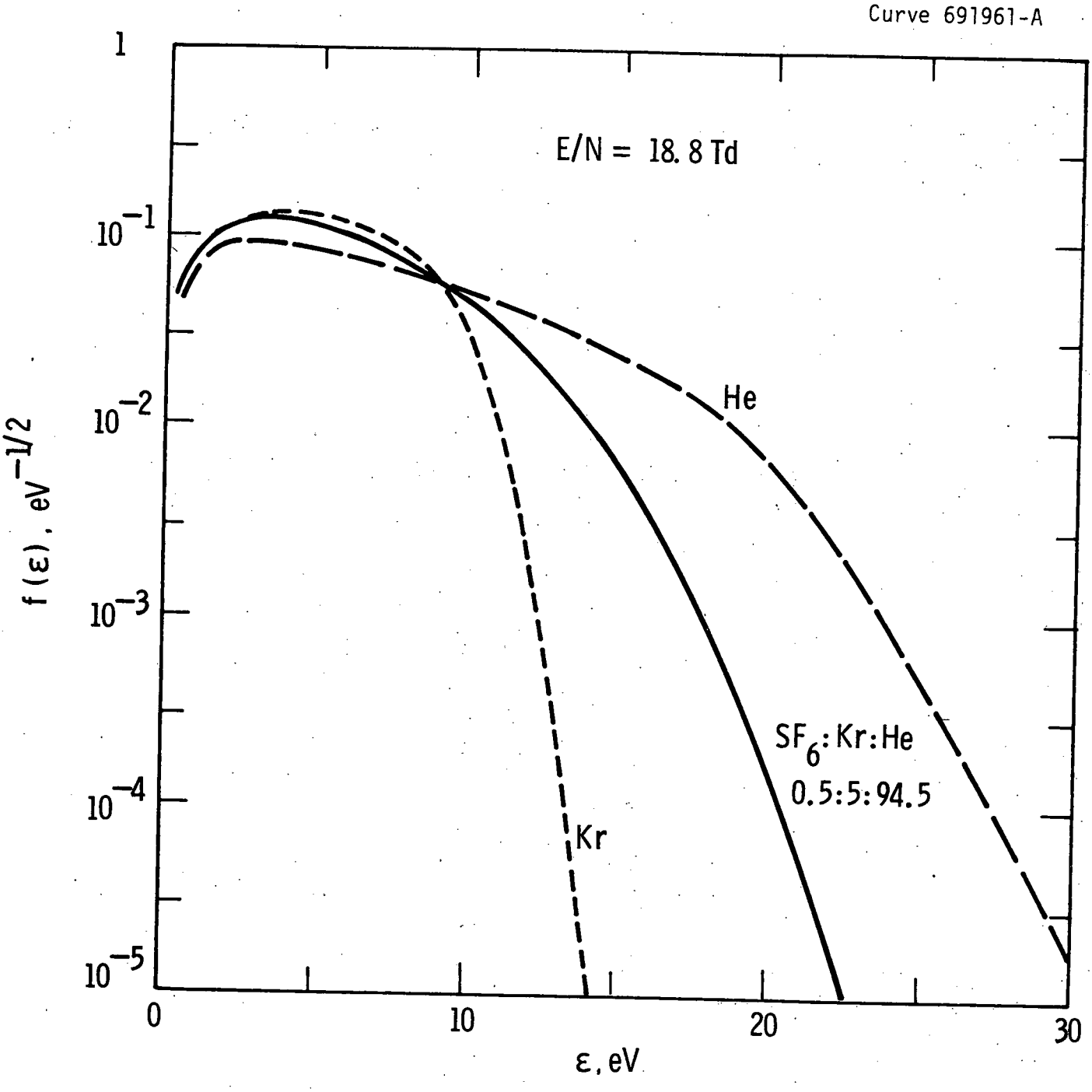


Fig. 4. Electron energy distributions in krypton, in helium, and in a $He:Kr:SF_6$ = 94.5:5:0.5 mixture.

$$\alpha_*/N = A \exp [-B (E/N)^{-1}] \quad (1)$$

and

$$\alpha/N = C \exp [-D (E/N)^{-1}] \quad . \quad (2)$$

The results also show that the total dissociative attachment coefficient, $\alpha_a/N$, and the electron drift velocity, W, can be fitted with functions of the form

$$\alpha_a/N = R (E/N)^{-S} \quad (3)$$

and

$$W = T (E/N)^{U} \quad . \quad (4)$$

Values of the curve-fit coefficients are summarized for three $He:Kr:SF_6$ mixtures in Table III. The value of $\alpha_2/n^*$, the coefficient for ionization of Kr*, was approximately equal to $1.6 \times 10^{-14}$ $cm^2$ over the range of E/N values of interest for the discharge calculations. The rate coefficients for excitation of Kr, ionization of ground state species, and attachment are related to the corresponding $\alpha$ coefficients by equations of the form

$$k\ (cm^3\ s^{-1}) = \nu/N = (\alpha/N)\ W \quad , \quad (5)$$

where k is the rate coefficient and $\nu$ is the corresponding collision frequency. The rate coefficient for two-step ionization (ionization of Kr*) is given by

$$k_2\ (cm^3\ s^{-1}) = \nu_2/n^* = (\alpha_2/n^*)\ W \quad . \quad (6)$$

The collision frequencies $\nu_*$, $\nu_i$, and $\nu_a$ and the rate coefficients $k_2$ appear in the equations which describe the densities of the various charged and excited species in the discharge.

Discharge Operating Characteristics for $He:Kr:SF_6$ Mixtures

The steady state and time dependent operating characteristics of glow discharges in $He:Kr:SF_6$ mixtures, and other mixtures of rare

Table III. Curve-fit coefficients for the calculation of $\alpha_*/N$, $\alpha/N$, $\alpha_a/N$ and W in three He:Kr:$SF_6$ mixtures. The values of A, C, and R have been multiplied by $10^{17}$. The value of T has been multiplied by $10^{-5}$.

| He:Kr:$SF_6$ | A | B | C | D | R | S | T | U |
|---|---|---|---|---|---|---|---|---|
| 94.5:5:0.5 | 3.25 | 22.9 | 3.50 | 50.2 | 9.44 | 1.37 | 1.85 | 1.00 |
| 89.5:10:0.5 | 4.00 | 23.6 | 3.40 | 57.8 | 7.64 | 1.27 | 2.40 | 0.892 |
| 84.5:15:0.5 | 4.00 | 25.3 | 3.70 | 67.1 | 4.43 | 1.21 | 2.30 | 0.875 |

gases and halogen-bearing compounds, can be predicted by formulating a set of rate equations for the densities of charged and excited species in the positive column of the discharge. The equations formulated here assume that the particle densities are uniform in the high pressure positive column. Steady state solutions of the rate equations result in a prediction of the steady state electric field in the positive column as a function of current density since the rate coefficients for electron-heavy particle reactions depend on E/N as discussed in the previous section.

The formulation is based on the electron energy balance calculations just described, previously published discharge modeling calculations,[14] and published rate coefficients. The following rate equations were formulated to model discharges in the $He:Kr:SF_6$ mixtures.

$$\frac{dn_e}{dt} = \nu_i n_e + k_2 n_e n^* - \nu_a n_e - k_r n_e n_+ \tag{7}$$

$$\frac{dn^*}{dt} = \nu_* n_e - k_d [SF_6] n^* - k_2 n_e n^* \tag{8}$$

$$\frac{dn_-}{dt} = \nu_a n_e - k_{ii} n_+ n_- \tag{9}$$

$$\frac{dn_+}{dt} = \nu_i n_e + k_2 n_e n^* - k_r n_e n_+ - k_{ii} n_+ n_- \tag{10}$$

In Eqs. (7)-(10) $n_e$, $n^*$, $n_-$, and $n_+$ are, respectively, the densities of electrons, excited krypton atoms, negative ions, and positive ions, and $[SF_6]$ is the $SF_6$ number density. The frequencies for excitation of krypton, ionization of all ground state species (one-step ionization), and dissociative attachment to $SF_6$ are, respectively, $\nu_*$, $\nu_i$, and $\nu_a$, while $k_2$ is the rate coefficient for ionization of Kr* (two-step ionization). The remaining rate coefficients which appear in Eqs. (7)-(10) $k_r$, $k_{ii}$, and $k_d$, are, respectively, the coefficients for electron-ion recombination, ion-ion recombination, and deactivation of Kr* by $SF_6$. The values assumed for these coefficients are taken from the literature and are listed in Table IV.

Table IV. Rate coefficients for electron-ion and ion-ion recombination and Kr* deactivation by $SF_6$. $X^-$ represents any possible negative ion produced from $SF_6$.

| Process | Rate Coefficient ($cm^3 sec^{-1}$) | Reference |
|---|---|---|
| $e + Kr_2^+ \rightarrow 2Kr$ | $k_r \approx 1 \times 10^{-7}$ | 33 |
| $X^- + Kr^+ \rightarrow XKr$ | $k_s = 1 \times 10^{-6}$ | 34 |
| $Kr^* + SF_6 \rightarrow$ products | $k_d = 1.8 \times 10^{-10}$ | 35 |

The removal of $SF_6$ can be calculated by adding a fifth rate equation:

$$\frac{d[SF_6]}{dt} = - k_a [SF_6] n_e \qquad (11)$$

where the dissociative attachment term has been rewritten to explicitly account for the dependence $\nu_a = k_a [SF_6]$. However, numerical calculations show that removal of $SF_6$ is negligible for the conditions of the present experimental studies. Therefore, Eq. (11) is not included in the model discussed here.

The four coefficients $\nu_*$, $\nu_i$, $k_a$, and $k_2$ all depend on E/N and n*/N as described in the preceding section. However, the n*/N dependence is weak as long as $n^*/N \lesssim 6 \times 10^{-5}$ as shown in Fig. 3. Therefore, the dependence of these coefficients upon n*/N has been ignored in solving Eqs. (7)-(10).

Time dependent and steady state solutions of Eqs. (7)-(10) have been obtained by using a simple series-resistor circuit equation to relate the discharge current density due to electrons,

$$j = n_e q_e W, \qquad (12)$$

to the value of E/N in the discharge positive column, where $q_e$ is the electronic charge. The circuit equation is

$$I = jA = [V_s - (E/N)Nd]R^{-1} \quad , \qquad (13)$$

where A is the discharge area, d is the discharge gap length, $V = (E/N)Nd$ is the positive column voltage, $V_s$ is the power supply voltage, and R is the series resistance. Cathode and anode sheath voltages are neglected in Eq. (13). The gas density is given by

$$N = 3.54 \times 10^{16} (273\ p/T)\ cm^{-3} \quad , \qquad (14)$$

where p is the pressure in Torr and T is the temperature in °K.

The error introduced by neglecting ion currents can be evaluated by solving Eq. (9) to find the steady state value of $n_-/n_e$. Note that addition of Eqs. (7) and (9) shows that $dn_e/dt + dn_-/dt = dn_+/dt$. Hence, if $n_- + n_e = n_+$ at $t = 0$ then $n_- + n_e = n_+$ for all $t > 0$. If this equality is used to eliminate $n_+$ from Eq. (9), then the steady state value of $n_-/n_e$ is

$$(n_-/n_e)_o = 0.5(\sqrt{1 + (4\nu_a/k_{ii}n_{eo})} - 1) \quad . \tag{15}$$

Equation (15) shows that $(n_-/n_e)_o$ increases as j and $n_{eo}$ decrease. The numerical solutions give $(n_-/n_e)_o = 10$ at $j = 0.1$ A/cm$^2$, the smallest current density considered.

The corresponding ion currents can be estimated by comparing the electron and ion mobilities. The unknown mobility, $\mu_2$, of $SF_6$ ions in He can be estimated from the known mobility, $\mu_1$, of $SF_6$ ions in $SF_6$ by using the expression[36]

$$\mu_2 = (m_1^{-1} + m_2^{-1})^{1/2}(m_2^{-1} + m_2^{-1})^{-1/2}\,\mu_1 \quad , \tag{16}$$

where $m_1$ is the mass of He and $m_2$ is the mass of $SF_6$, $SF_6^-$, and $SF_6^+$. Evaluation of Eq. (16) with[37] $\mu_1 = 0.55$ cm$^2$/volt sec gives $\mu_2 = 2.4$ cm$^2$/volt sec. The electron mobility is determined from the results of the previous section to be $\mu_e = 690$ cm$^2$/volt sec. Hence

$$\frac{W_+}{W} \approx \frac{W_-}{W} \approx \frac{\mu_2}{\mu_e} = 3.5 \times 10^{-3} \quad . \tag{17}$$

The total current density including the contributions from the positive and negative ions is

$$j_{total} = n_e q_e W \left(1 + \left[\left(\frac{n_-}{n_e}\right)_o + 1\right]\frac{W_+}{W} + \left(\frac{n_-}{n_e}\right)_o \frac{W_-}{W}\right) \quad . \tag{18}$$

Substitution of the numerical value of $W_+/W \approx W_-/W$ from Eq. (17) and $(n_-/n_e)_o = 10$ gives $j_{total} = 1.07\, j_e$, i.e., an error of only 7%. This error

rapidly decreases as $j_e$ increases. Furthermore, the numerical solutions of Eqs. (7)-(10) and (13) show that at low values of $j_e$ ($\lesssim$0.3 A/cm$^2$) the steady state solution of Eq. (7) requires that $\nu_i = \nu_a$, which implies that the positive column E/N has a constant value, independent of current density. Thus a flat E/N-j characteristic is predicted at low current densities whether or not ion currents are considered. Since the ion current is negligible compared with the total current density except at low current densities where E/N is independent of j, we have neglected ion currents in the calculation of the E/N-j characteristics.

The discharge formation time predicted by Eqs. (7)-(10) and (13) decreases as the applied voltage increases. The calculated discharge formation time for a He:Kr:$SF_6$ = 94.5:5:0.5 mixture decreases from 30 nsec to 15 nsec as the applied voltage is increased from $3V_{ss}$ to $5V_{ss}$, where $V_{ss}$ is the steady state positive column voltage. This range of applied voltages approximately corresponds to the range of applied voltages used in the experiments to be described. These calculated discharge formation times are much shorter than the duration of the experimental current pulses, so that the experimental discharges will reach steady state conditions. Therefore, the following is concerned with the prediction of steady state discharge operating characteristics.

Steady-State Discharge Characteristics

The numerical solutions of Eqs. (7)-(10) and (13) show that the recombination term in Eq. (10) does not become important until the value of $(n_-/n_e)_o$ is small and $n_+ \approx n_e$. Substituting $n_+ = n_e$ into Eq. (7) and neglecting ion currents, we get a simplified positive column model which consists of Eqs. (7) and (8) only. The steady state values of $n_e$ and n*, and the positive column E/N-j characteristic are obtained by analytically solving Eqs. (7) and (8).

The E/N-j characteristic calculated for a He:Kr:$SF_6$ = 94.5:5:0.5 mixture is shown in Fig. 5 for two cases. The curve labeled "with recombination" uses $k_r = 1.1 \times 10^{-7}$ cm$^3$ sec$^{-1}$, while the curve labeled "without recombination" uses the value $k_r = 0$. These curves are only qualitative for $j \gtrsim 10$ A/cm$^2$, where $n^*/N > 6 \times 10^{-5}$ and the rate coefficients are no longer functions of E/N only. The E/N-j characteristic is independent

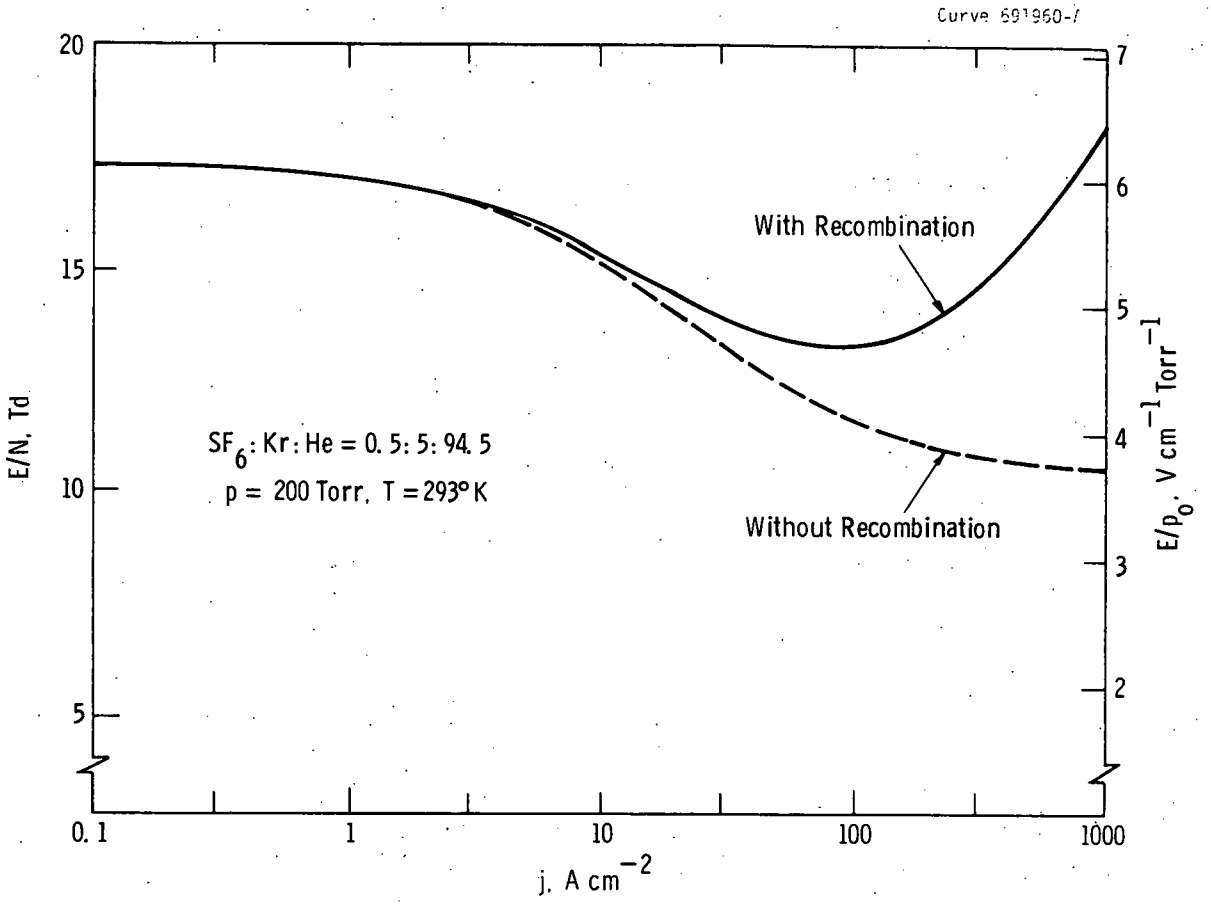


Fig. 5. Calculated E/N vs. j characteristics for a He:Kr:$SF_6$ = 94.5:5:0.5 mixture.

of j at low current densities $j \lesssim 0.3$ A/cm$^2$, as discussed above, because E/N is determined by a balance between one-step ionization and attachment. E/N decreases as j increases beyond $\sim$0.3 A/cm$^2$ because two-step ionization becomes an important electron production process. At high current densities $j \gtrsim 100$ A/cm$^2$ almost all of the Kr* produced is ionized, and this ionization process is the dominant electron production process. In this high current density regime the ionization rate is equal to the Kr* production rate, and ionization appears as a one-step process. When $k_r = 0$ the E/N-j characteristic is flat in this regime since attachment becomes the dominant electron loss process. When $k_r = 1.1 \times 10^{-7}$ cm$^3$ sec$^{-1}$, recombination dominates, and E/N increases as j increases.

Further information about the one-step ionization rate $R_1 = \nu_i n_e$, the two-step ionization rate $R_2 = k_2 n^* n_e$, the attachment rate $R_a = \nu_a n_e$, and the recombination rate $R_r = k_r n_e^2$ is given in Fig. 6 in the form of curves of $R_2/R_1$ vs. j and $R_r/R_a$ vs. j.

If attention is restricted to the current density range $0.1 \leq j \leq 10$ A/cm$^2$ then recombination can be neglected and the simultaneous solution of Eqs. (7) and (8) with $dn_e/dt = dn^*/dt = 0$ yields

$$n_{eo} = [k_d[SF_6](\nu_i - \nu_a)][k_2(\nu_i + \nu_* - \nu_a]^{-1} \qquad (19)$$

and

$$n_o^* = (\nu_* n_{eo})(k_2 n_{eo} + k_d[SF_6])^{-1} \quad . \qquad (20)$$

The corresponding steady state current is given by Eq. (12). The E/N vs. j characteristics predicted by Eqs. (19) and (12) are given in Fig. 7 for two He:Kr:$SF_6$ mixtures at three pressures. The pressure dependence arises from the $[SF_6]$ term in Eq. (19) and the assumption of constant mixture proportions.

The E/N-j curves shown in Fig. 7 correspond to the conditions studied experimentally. These curves are compared with experiment in Section III. The calculated values of E/N are higher in the mixture containing 15% Kr, compared with the values of E/N in the mixture containing 5% Kr, because an increase in the amount of Kr in the mixture increases the relative number of low energy electrons and the resulting attachment

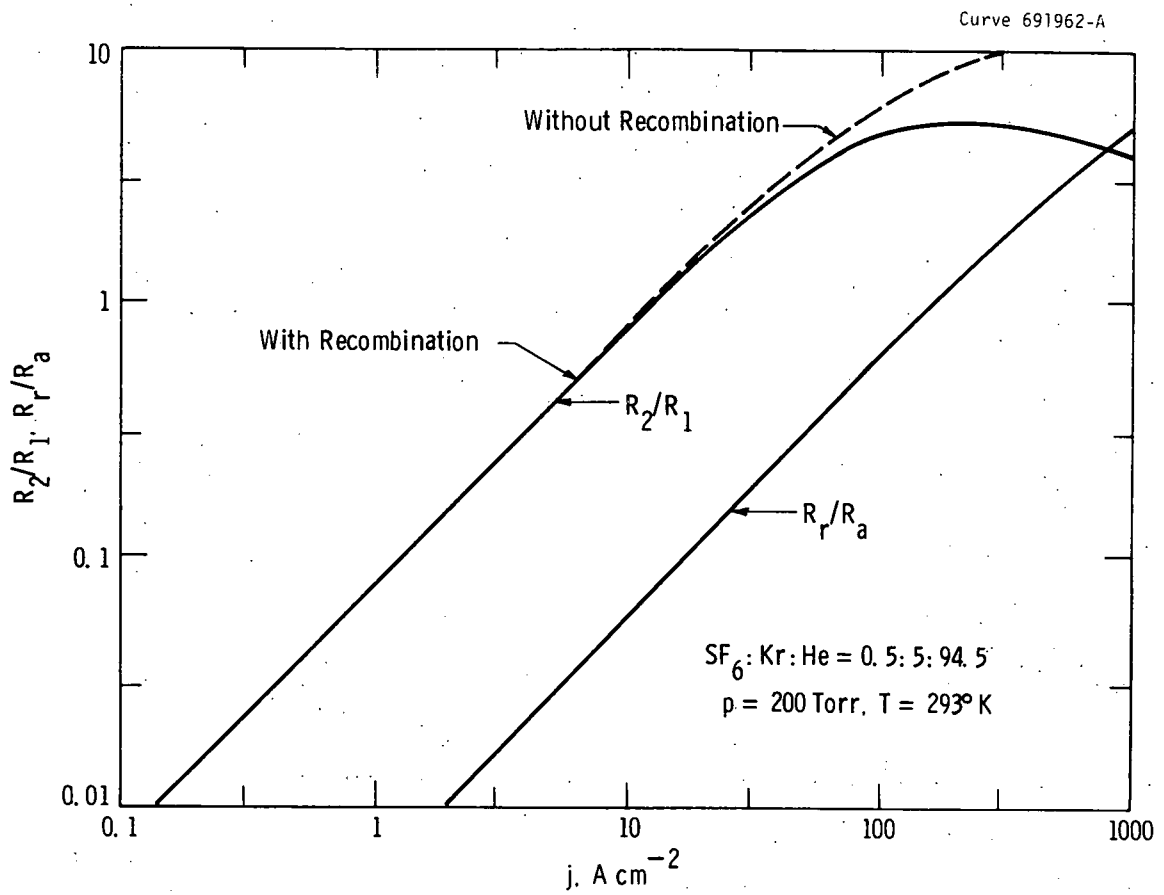


Fig. 6. Calculated curves of $R_2/R_1$, the ratio of the two-step and one-step ionization rates, and $R_r/R_a$, the ratio of the recombination rate and the attachment rate, vs. current density for the same conditions as Fig. 5.

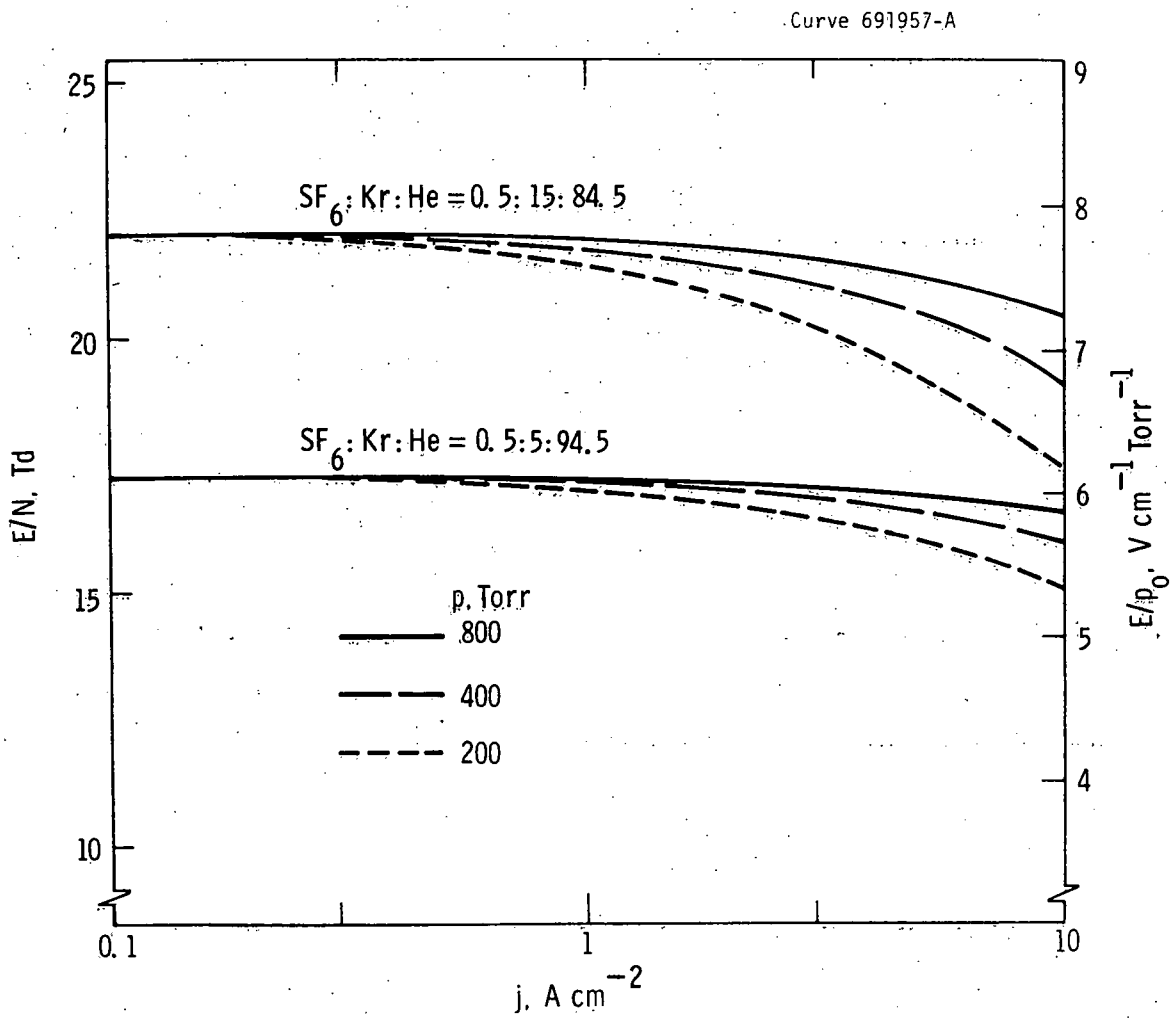


Fig. 7. Calculated E/N-j characteristics for two different He:Kr:$SF_6$ mixtures and three pressures.

rate. Hence, a higher E/N is required for steady state discharge operation. The highest experimental current density was about $j = 2$ A/cm$^2$ at 200 Torr. At this current density and pressure Fig. 6 gives $R_2/R_1 = 0.15$, indicating that two-step ionization is an important electron production process. The values of electron density $n_e$ and fractional ionization $n_e/N$ are approximately proportional to the current density. At $j = 2$ A/cm$^2$, we have $n_e = 4 \times 10^{12}$ cm$^{-3}$ and $n_e/N = 6 \times 10^{-7}$.

## B. Discharge Stability

Instabilities in diffuse laser glow discharges can generally be divided into two categories: those that may be tolerated or easily controlled and those that may impose severe limitations on discharge maintenance. For example, striations, oscillations, or a tendency toward relatively mild, large-scale constriction are usually not as serious as the glow-to-arc transition, which can terminate laser operation catastrophically. Various discharge stability analyses have been formulated to guide the development of useful lasers. In some cases the analyses have turned out to describe relatively mild instabilities rather than important obstacles to laser operation. In order to determine the significance of a stability analysis, it is important to identify how the corresponding instability manifests itself experimentally.

An example of an apparently controllable instability is that discussed by Daugherty, Mangano, and Jacob[38] in a paper concerned with an electron beam-controlled, rare gas-halogen laser discharge. That analysis results in a stability criterion which implies that an external ionization source is required for stable operation and that self-sustained steady-state operation of such a discharge is impossible. It appears, however, that the instability of concern is simply a bulk effect corresponding to the discharge current-voltage characteristic being negative--an instability which is easily stabilized with an external ballast impedance in the circuit. This conclusion is supported by experimental results of the present study. The original stability analysis and its generalization for the present study proceed as follows.

The reported stability criterion[38] results from the continuity equations for electrons and metastables, which describe electron production

by electron beam ionization and two-step electron-impact ionization and electron loss by attachment. These equations are, respectively,

$$\frac{dn_e}{dt} = S_{eb} + \nu_2 n_e - \nu_a n_e \qquad (21)$$

and

$$\frac{dn^*}{dt} = k^* n_g n_e - \frac{n^*}{\tau_d} - \nu_2 n_e \quad , \qquad (22)$$

where $n_e$ is the electron density, $S_{eb}$ is the electron production rate resulting from a high-energy electron beam, $\nu_2$ is the ionization frequency for metastable noble gas atoms, $\nu_a$ is the attachment frequency, $n^*$ is the metastable density, $k^*$ is the rate coefficient for production of metastables by electron impact, $n_g$ is the ground-state atom density, and $(\tau_d)^{-1}$ is the loss rate of the metastables by processes other than electron-impact ionization. Since only two-step ionization is considered, $\nu_2$ equals $k_2 n^*$, where $k_2$ is the rate constant for production of electrons by collisions of electrons with metastables. The stability criterion results from a linearized analysis of perturbations in electron density and metastable density from their steady-state values, with the discharge electric field held constant in time. The discharge is assumed to be spatially uniform.

Note that the last term in Eq. (22) has been added to the equations of Ref. 38 in order to make the pair of equations self-consistent. With this additional term, the linearized perturbation analysis of Ref. 38 yields the stability criterion

$$\nu_a \geq 2\nu_{2o} - \tau_d k_2 S_{eb} \quad , \qquad (23)$$

where $\nu_{2o}$ is the steady-state ionization frequency. This criterion differs from the published criterion by the second term on the right of the inequality sign. Thus, the new term in Eq. (22), which accounts for the loss of metastables by ionization, helps to some extent to stabilize the system.

For self-sustained operation Eq. (23) gives $\nu_a \geq 2\nu_{2o}$. This criterion is clearly incompatible with the steady-state condition described by $\nu_a = \nu_{2o}$, and it seems to be inconsistent with the formation or maintenance of a steady-state self-sustained discharge. As indicated above, however, it appears that this criterion does not correspond to a significant instability such as the glow-to-arc transition, but rather to the over-all voltage-current characteristic. This interpretation is supported by the results of the present study as well as by the following experimental and theoretical observations.

Daugherty, Mangano, and Jacob[38] describe the experimental manifestation of the onset of the instability as a volumetric growth in current. These observations are clarified by Daugherty,[39] who points out that "the discharge current "took off" after initially tending toward the expected equilibrium value. Observations under lasing conditions suggested that the discharge current was not constricting to an arc, but that (at least initially) a large volume of the discharge was unstable". These reports clearly indicate a spatially distributed growth in total current rather than an internal redistribution of current density[1,8,9] within the diffuse plasma. Thus, the instability appears not to involve spatial nonuniformities and filamentation,[1,8,9] as are associated with the glow-to-arc ionization instability. (If, of course, this instability in the total current were allowed to develop, it would eventually lead to other instabilities, inhomogeneities, and arc formation.)

An analogy can be made between the theory for the laser discharge and that for a conventional low-pressure fluorescent lamp glow discharge.[40] That discharge is also dominated by two-step ionization, and although electron loss is by diffusion rather than by attachment, the loss rate is similarly linear in $n_e$. Thus, the electron continuity equation can be expressed in a form identical to Eq. (21) with $S_{eb} = 0$. Thus, a perturbation analysis of the type discussed would predict that the lamp discharge is unstable. Indeed, it is. However, the instability manifests itself experimentally simply as a spatially distributed growth in the total current, which is easily stabilized with an external ballast impedance in the discharge circuit. In this case the stability criterion

indicates that the fluorescent lamp V-I characteristic is negative. Thus, the criterion may be considered to be a condition for achieving stability by means of internal ballasting (e.g., with e-beam ionization) instead of external ballasting.

The experimental results of the present study can be related to the instability of Ref. 38 if Eq. (21) is modified to include single-step ionization. The experimental results of this study correspond to self-sustained operation ($S_{eb} = 0$) with the current density in the range $0.1 \leq j \leq 10$ A/cm$^2$. As indicated previously, for this current density range the rate equations for the electrons and metastables can be written, respectively,

$$\frac{dn_e}{dt} = \nu_1 n_e + k_2 n^* n_e - \nu_a n_e \qquad (24)$$

and

$$\frac{dn^*}{dt} = \nu_* n_e - \frac{n^*}{\tau_d} - k_2 n^* n_e \quad , \qquad (25)$$

where $\nu_1$ is the single-step ionization frequency and where we still have $\nu_2 = k_2 n^*$.

The effect of single-step ionization can be incorporated into the stability criterion, Eq. (23), quite easily, since the process is linear in $n_e$. Mathematically, the presence of the single-step ionization term in Eq. (24) simply alters the coefficient of the term already linear in $n_e$ in Eq. (21), and the new stability criterion is obtained by replacing $\nu_a$ in Eq. (23) by $(\nu_a - \nu_1)$. The resulting stability criterion, with $S_{eb} = 0$, is

$$\nu_a \geq \nu_1 + 2\nu_{2o} \quad . \qquad (26)$$

Again, this criterion is incompatible with the steady-state condition $\nu_a = \nu_1 + \nu_{2o}$. Thus a demonstration of steady-state discharge operation would violate this criterion and would show that the instability represented by Eq. (23) or Eq. (26) is not a significant limitation to discharge operation.

The initial growth rate of the instability represented by Eqs. (23) and (26) is characterized by the time $\tau$ given by

$$\tau = \frac{1}{a}\left(\sqrt{1-\frac{b}{a^2}} - 1\right)^{-1} \quad , \tag{27}$$

where

$$a = \frac{1}{2}\left(\frac{1}{\tau_d} + k_2 n_{eo} - \nu_1 - \nu_{2o} + \nu_a\right) \tag{28}$$

and

$$b = -\frac{1}{\tau_d}(\nu_1 + 2\nu_{2o} - \nu_a) + k_2 S_{eb} \quad , \tag{29}$$

and where $n_{eo}$ is the steady-state electron density. Note that Eqs. (27)-(29) include the effects of single-step electron impact ionization and ionization by a high-energy electron beam. In this case the steady-state electron continuity equation is

$$S_{eb} + (\nu_1 + \nu_{2o} - \nu_a)n_{eo} = 0 \quad . \tag{30}$$

Values of the characteristic time $\tau$ have been calculated for the experimental discharges established in the present study. In this case $S_{eb} = 0$, and we have

$$a = \frac{1}{2}\left(\frac{1}{\tau_d} + k_2 n_{eo}\right) \tag{31}$$

and

$$b = -\frac{\nu_{2o}}{\tau_d} \quad . \tag{32}$$

Note that the single-step ionization frequency does not appear explicitly in the expression for $\tau$. The calculated values of $\tau$ are discussed with the experimental results.

# III. EXPERIMENT

## A. Discharge System

### General System Layout

A general view of the experimental discharge system developed for this study is shown in the photograph of Fig. 8. The gas handling system is housed in the closed rack shown at the left side of the figure. The high voltage power supplies and electronic timing circuitry are located under the table. The discharge chamber and its associated electronic components, i.e., pulse forming network, trigger generators, spark gaps, etc., are positioned on the central portion of the table. A large rectangular metal box is used to cover these components. This box provides electrical shielding for scopes and other diagnostic equipment and, with a vent system (not shown) acts as a fume hood to prevent escape of gases. Plexiglas front and rear panels are available for the gas-handling rack to prevent the release of gas into the laboratory. A vent system is available to remove gas released inside the rack.

### Discharge Chamber

The discharge chamber was designed with relatively small dimensions and with circular symmetry so that changes in electrode structure or configuration could be implemented without major effort or expense. The chamber is shown schematically in Fig. 9. The cylindrical side wall is machined from solid Lexan. It has nominal dimensions of 8 1/2 in. I.D. by 12 in. O.D. by 10 in. high. The top flange was initially constructed of Lexan, but was later replaced with stainless steel. The bottom flange, which contains the gas inlet and exhaust ports and the high voltage feed-through for the preionizer assembly, is fabricated of stainless steel. The viewing windows in the side wall are calcium fluoride or MgO coated quartz mounted in stainless steel flanges. Teflon O-Rings are used for sealing all flanges to the Lexan side wall.

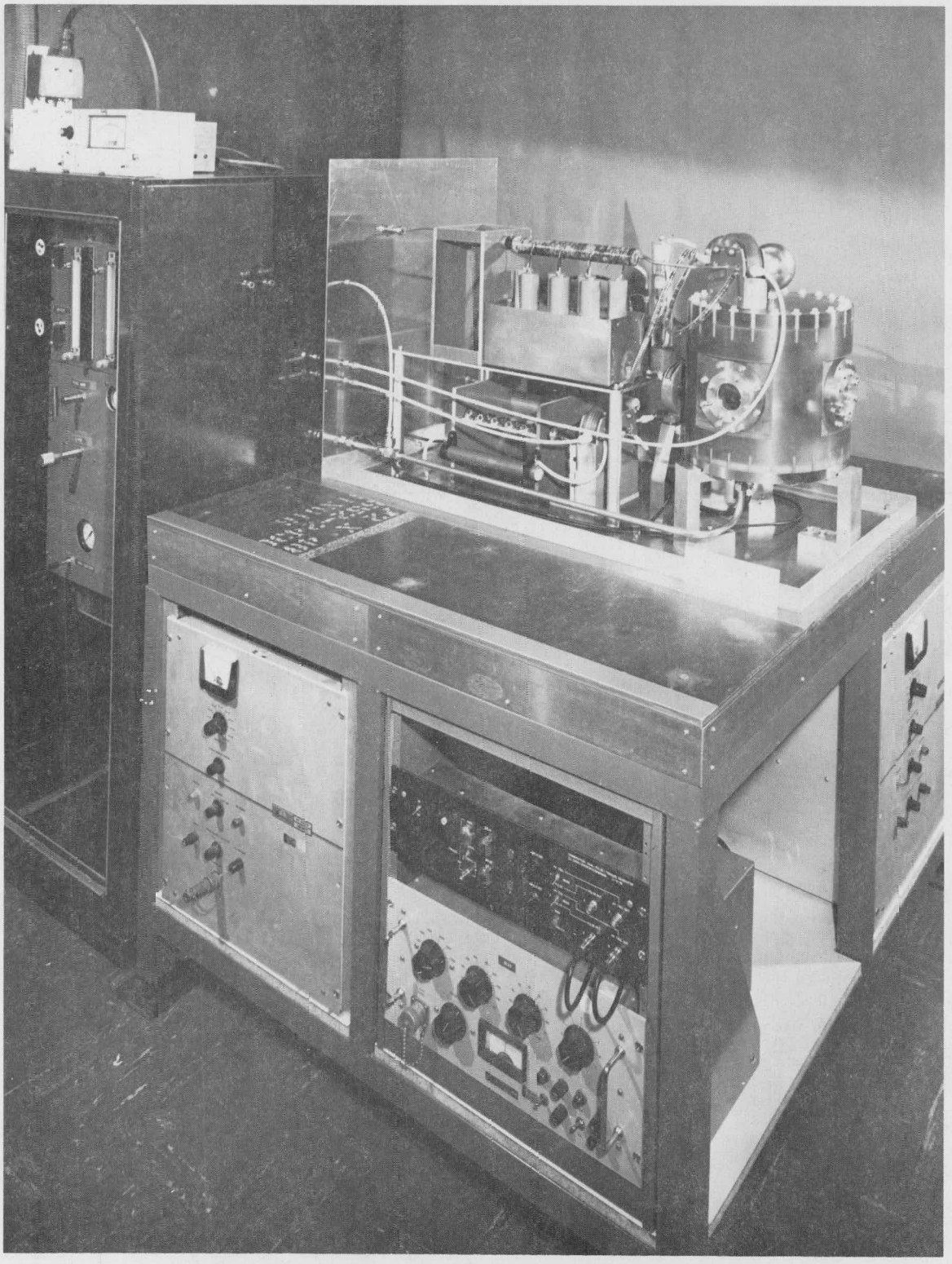

Fig. 8. Photograph of the experimental system.

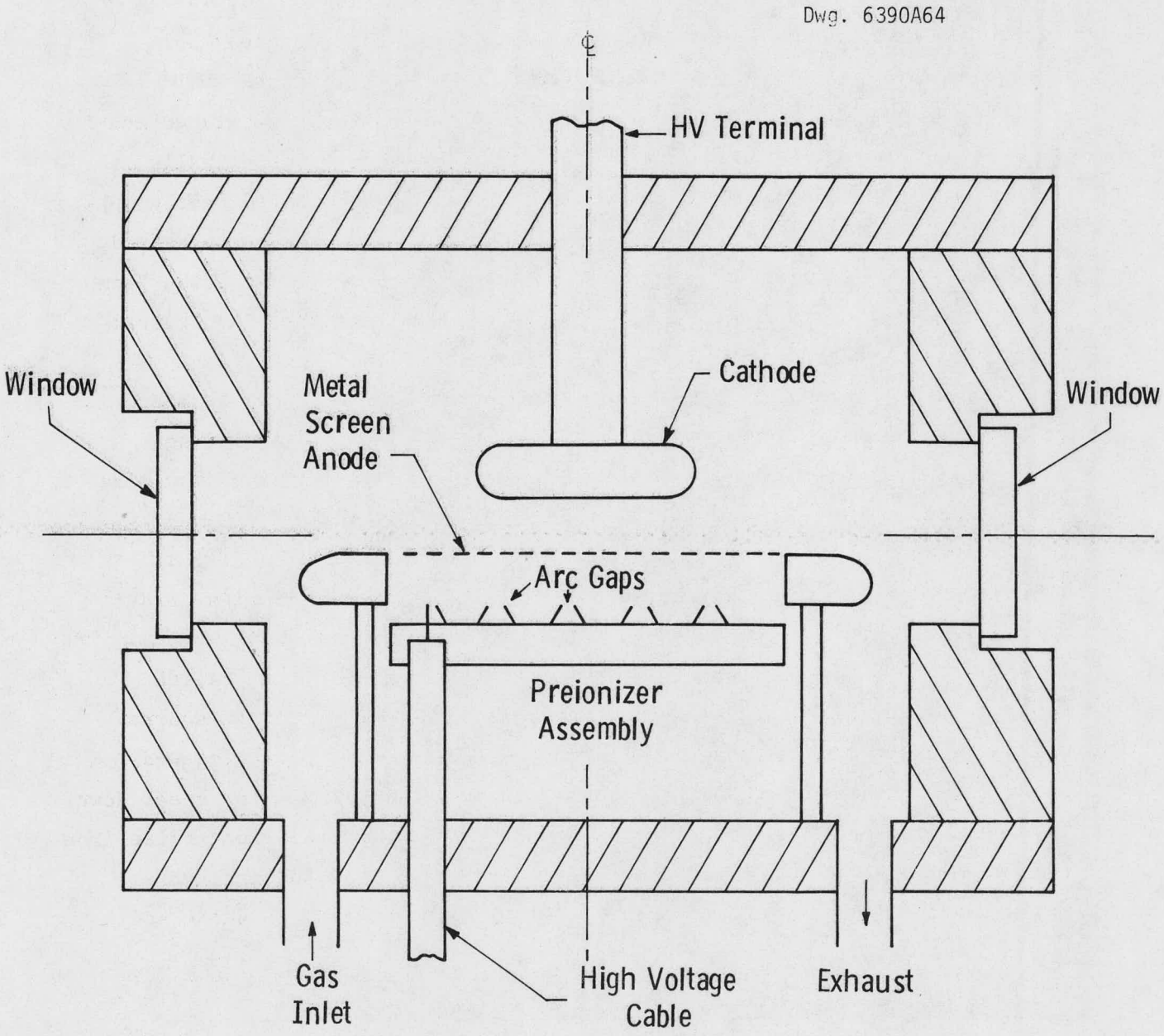


Fig. 9. Diagram of the discharge chamber.

The anode and cathode electrodes are fabricated of stainless steel; they are circular in cross section. The central section of the anode is a flat, stretched stainless steel screen which permits uv radiation from the preionizer to enter the discharge region. This screen is nominally 40 mesh with a transmission of approximately 55%. The stainless steel cathode has a convex profile to facilitate the development of uniform discharges. This profile, which is tabulated and shown in cross section in Fig. 10, has been determined experimentally in previous studies conducted at the Westinghouse R&D Center. Photographs of the anode and cathode are shown in Fig. 11. A metal mask was located just under the stainless mesh of the anode to limit the uv radiation from the preionizer to a 2 in. diameter cylindrical section under the central portion of the cathode. The threaded cylinder attached to the back of the cathode extends through the top flange of the discharge chamber to provide a high voltage connection. The anode-cathode gap spacing is changed by rotating the threaded cylinder and thus raising or lowering the cathode.

The preionizer assembly, located under the anode in Fig. 9, is constructed on a circular Lexan base. It consists of a series array of small arc gaps located in a back-and-forth groove milled in the Lexan, as shown in the isometric sketch of Fig. 12. The high voltage cable from the pulse voltage source is attached to one end of this array while the other end is grounded through a circular metal plate located under the Lexan base. When a voltage pulse is applied, the gaps break down in sequence until they are all conducting. Then the main current pulse from the power source flows through the gaps, producing arcs and the uv radiation required for ionization of the main gap between the anode and cathode.

Gas Handling System

The gas handling system is shown schematically in Fig. 13. The system was designed for possible use with corrosive gases such as fluorine. Thus, all parts of the system that may be exposed to such gases as fluorine, or fluorine-bearing gases, is constructed of stainless steel. Each gas is metered into the system by a rotomator type flow meter that

Dwg. 6419A08

| r inches | z inches |
|---|---|
| 0 | 0 |
| 0.15 | 0 |
| 0.25 | 0.0005 |
| 0.35 | 0.0015 |
| 0.45 | 0.0035 |
| 0.55 | 0.0055 |
| 0.65 | 0.0080 |
| 0.75 | 0.0105 |
| 0.85 | 0.013 |
| 0.95 | 0.0155 |
| 1.05 | 0.018 |
| 1.15 | 0.023 |
| 1.25 | 0.036 |
| 1.35 | 0.061 |
| 1.45 | 0.099 |
| 1.54 | 0.170 |
| 1.59 | 0.290 |
| 1.61 | 0.550 |

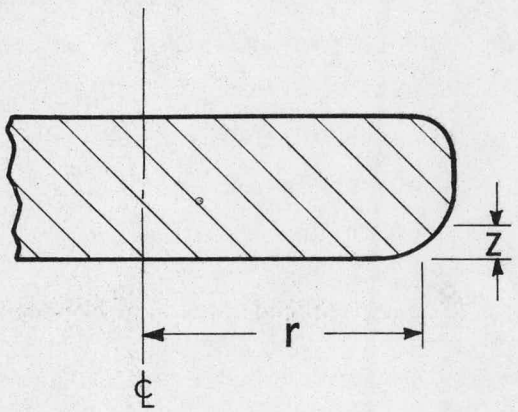


Fig. 10. Profile of cathode.


Fig. 11. Photograph of the anode (left) and cathode (right) used in the experimental studies.

Dwg. 6419A10

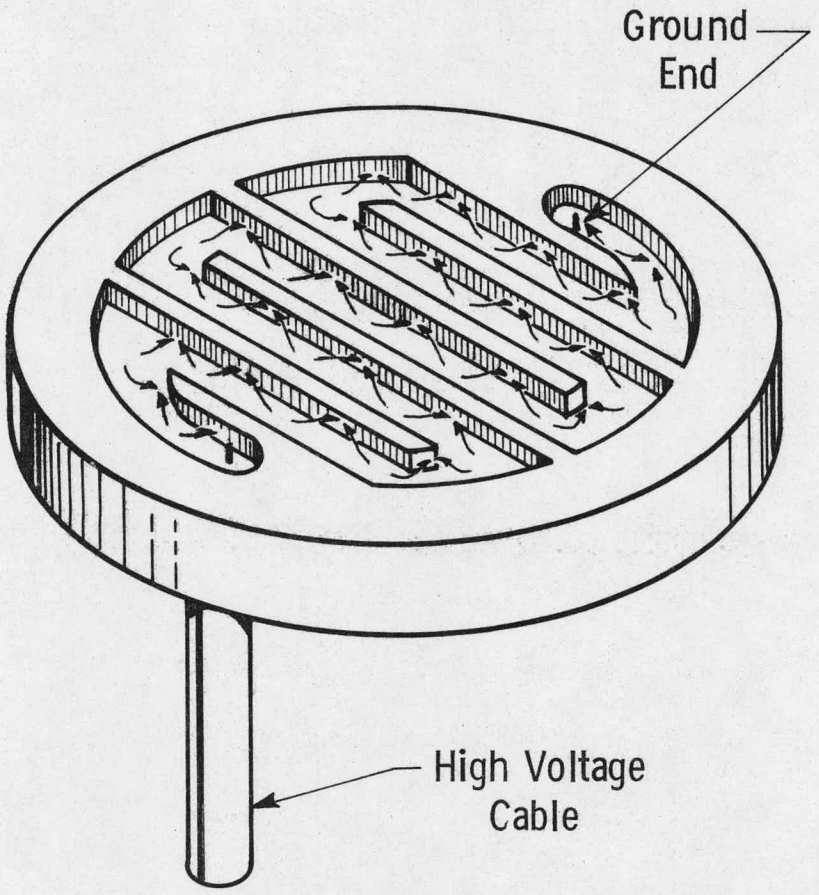


Fig. 12. Isometric drawing of preionizer assembly. The arc gaps are represented by the arrows facing each other. The actual assembly contained 13 grooves and 85 arc gaps.

Dwg. 6419A09

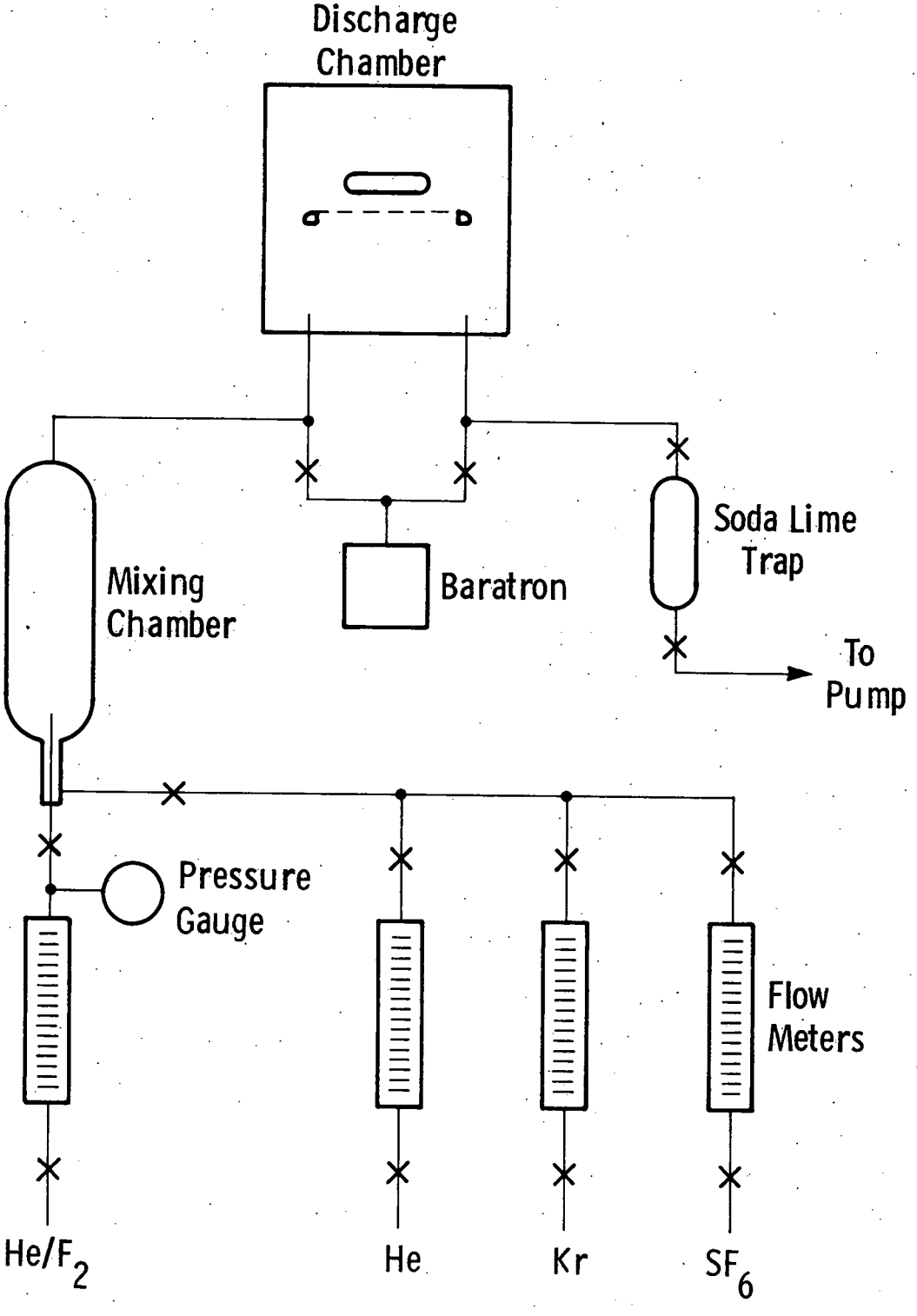


Fig. 13. Schematic drawing of gas handling system.

is calibrated for that gas. The non-corrosive gases used in these experiments, He, Kr, and $SF_6$, flow into a common manifold and then into a mixing chamber. The mixed gases are admitted into the system until the desired total pressure is achieved and then the gas flow is turned off. The pressure measurements in the discharge chamber are made with a special Baratron that is compatible with fluorine.

The discharge chamber and gas handling system are evacuated by a single mechanical pump. A soda-lime trap installed in the pump line is available to remove fluorine that would otherwise react with the pump oil. The exhaust of the pump is vented into a special exhaust system. This eliminates any possible exposure of personnel to fluorine that might get through the pump.

In initial experimental studies the gases were admitted into the discharge chamber one at a time starting with the minority constituents and finishing with the major constituent, helium.
This procedure is convenient, particularly when the concentration of the minor constituent is low, i.e., less than 1-2%. It does not, however, produce uniformly mixed gas in the discharge chamber. The gas handling procedure that was adopted was as follows. The flow rate for each gas was adjusted to provide the desired mixture while the valves to the pump were still open. After a time delay of a few minutes, which allowed the desired gas mixture to be established throughout the entire system, the pump valve was shut off and the pressure was allowed to build up in the discharge chamber. When the desired total pressure was reached, the valves to the gas supply system were closed.

It was necessary to apply a correction to the metered concentration of the minor constituent, say $SF_6$ (see Fig. 13). This correction was required to compensate for the $SF_6$ gas in the supply line from the $SF_6$ inlet to the junction with the next gas inlet. The $SF_6$ gas in this section of line builds up to the total pressure of the system but does not mix with the other gases in the discharge chamber. For example, in a binary He-$SF_6$ mixture it is necessary to meter in 0.2% $SF_6$ in order to have a 0.1% $SF_6$ concentration in the discharge chamber. Similarly 0.6%$SF_6$ must be metered in to achieve a 0.5% $SF_6$ concentration in the

mixture. In a triple mixture, say He:Kr:$SF_6$, the correction factors are much less since the volume of tubing occupied by unmixed $SF_6$ is less (see Fig. 13).

Electronics

Figure 14 shows a schematic view of the discharge chamber and the associated electronic components. The cathode C, screen anode A, preionizer P, and one of the three viewing windows W on the discharge chamber are shown. $HV_d$ is the high voltage power supply voltage used to charge the pulse-forming network, PFN. $R_d$ is the PFN charging resistance which protects the high voltage supply from arcs in the discharge; it has a value to give a short circuit current of 1 mA at 10 kV. Maxwell spark gap switches $SG_d$ for the discharge and $SG_p$ for the preionizer spark array require voltage-divider resistors $R_3$, $R_4$, $R_5$, and $R_6$ for proper trigger electrode operation. The spark gaps were triggered Tobe Deutschmann type TG-2 modules which were in turn triggered by two trigger generators, one delayed with respect to the other by an adjustable delay generator. The entire system was manually triggered by a single-shot multivibrator. $HV_p$ is a high voltage supply used to charge the energy storage capacitor $C_p$ for the preionizer spark array. $R_p$ is the charging resistance for $C_p$. Current transformers $CT_d$ and $CT_p$ monitor the discharge and preionizer spark array currents. Pr is a Tektronix high voltage probe for monitoring the cathode voltage of the discharge.

In most of our tests the energy storage capacitor $C_p$ for the preionizer spark array was charged to a voltage between 5 and 10 kV. In order to prevent arcing from the array to the underside of the anode structure the spark array was moved further from the anode than originally placed and dielectric barriers were installed. By observing the pattern of sparks reflected from the curved surface of the cathode it was possible to select a satisfactory operating voltage where all preionizer sparks were firing and no current was bypassed to the anode. For all data in this report the spark array was observed to operate in this manner. At the lower discharge gas pressures, 100 and 200 Torr, the spark array performed well at a charging voltage of 5 kV whereas at 400, 600, and 800 Torr the array worked better if the charging

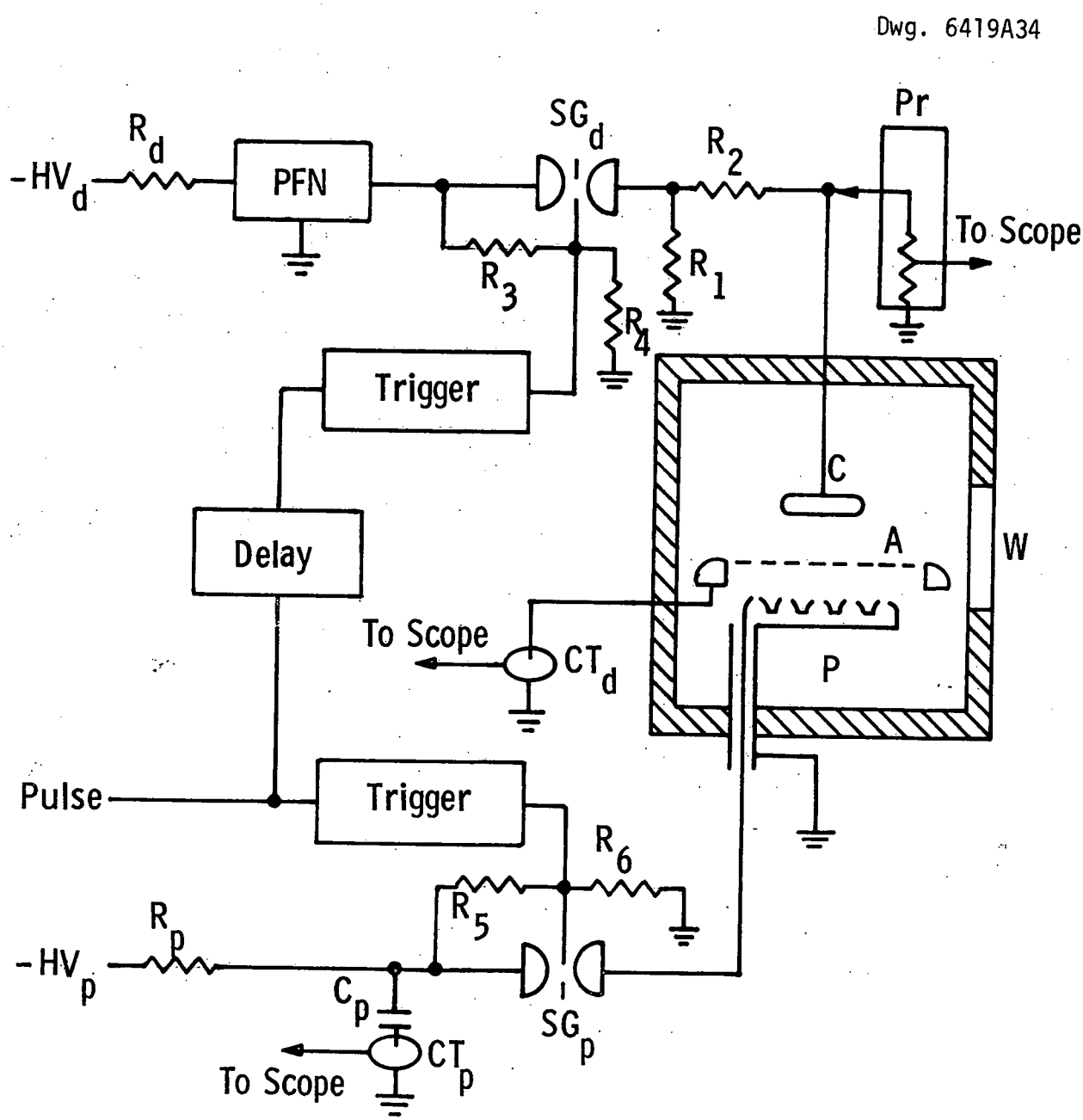


Fig. 14. Schematic diagram of the discharge chamber and circuitry.

voltage was increased somewhat. Current and voltage waveforms for the preionizer, obtained using current transformer $CT_p$ and a high voltage probe, yielded currents of about 100 A with a duration of about 200 nsec for $C_p$ = 2 nF. Under these conditions the energy in the preionizer discharge was 0.025 joule per pulse for a charging voltage of 5 kV and 0.1 joule per pulse for a charging voltage of 10 kV.

The pulse forming network was a seven-stage network which produced a 1 μsec pulse and had a characteristic impedance $Z_o$ of 70 Ω. The total capacitance in the PFN was 7 nF. Thus,with a charging voltage of 10 kV, the stored energy in the PFN was 0.35 joules. The delay between the firing of the preionizer discharge and the main discharge was varied to determine a satisfactory operating value. The delay for which minimum discharge arcing occurred was 0.1 μsec; this was the delay used for all data reported. The combination of $R_1$ and $R_2$ was used to terminate the PFN with approximately 70 Ω while ballasting the discharge with various resistances from 35 Ω to 2035 Ω. $R_1$ values of 70 Ω and 110 Ω were used. $R_2$ values of 2010, 710, 200, and 0 Ω were used to obtain glow currents from 1 A to 100 A. Values of $R_d$, $R_3$, and $R_4$ were, respectively, 10 MΩ, 100 MΩ, and 50 MΩ, which allowed the PFN to be charged to -0.94 $HV_d$.

Measurements of discharge current $I_d$ and discharge voltage $V_d$ were made using a Pearson current transformer ($CT_d$) and the high impedance Tektronix high voltage probe. The consistency of the measured values of $I_d$ and $V_d$ were checked using Ohm's law by means of the following equation.

$$V_d' = 0.94\ HV_d\ R_1/(R_1 + Z_o) - [Z_o R_1/(Z_o + R_1) + R_2]\ I_d \quad , \quad (33)$$

where $V_d'$ is the calculated value of discharge voltage. Measured values of discharge voltage $V_d$ differing from $V_d'$ by 3% or less were obtained. In order to fire the spark gap $SG_d$ reliably, values of $HV_d$ greater than 10 kV were required. Measurements made at 100 and 200 Torr yielded values of $V_d$ between 500 and 1500 V which were better tested for consistency using an equation for the calculated discharge current,

$$I_d' = [V_d - 0.94\ HV_d R_1/(R_1 + Z_o)]/[Z_o R_1/(Z_o + R_1) + R_2] \quad , (34)$$

which was compared with the measured discharge current $I_d$. This latter check avoided relying on differences of large numbers on the right hand side of Eq. (33).

## B. Measurements and Results

Measurements of discharge characteristics were made for the following conditions:

Gas mixture: $He:Kr:SF_6$ = 94.5:5:0.5
84.5:15:0.5

Total gas pressure: 100-800 Torr

Discharge gap (at center of cathode): 0.5, 1.48, 3.13 cm

Discharge current: ∿1-100 A

The gap variation permitted the positive column electric field to be separated from the sheath voltages for comparison with theory. Polaroid photographs were taken of the glows to determine discharge diameters so that cross-sectional areas and current densities could be estimated. Values of current density that are reported are average values based on the assumption that the current density is uniform within the cross-sectional area obtained from the photographs. The steady-state glow voltage is defined as that steady voltage existing after initiation of the glow when the current has reached a steady value prior to any transition to an arc. Measurements were also made of the duration of the steady glow, where the duration is taken to be the time during which glow voltage is constant as mentioned above.

Figure 15(a) shows a dual-beam trace of discharge voltage (upper curve) and current (lower curve) obtained in a glow discharge in a mixture of 0.5% $SF_6$, 5% Kr, and He. The pressure was 200 Torr, and the discharge gap was 3.13 cm. For Fig. 15(a) the power supply voltage $HV_d$ was 28 kV, $R_1$ was 70 Ω, and $R_2$ was 710 Ω. The network was nearly matched by $R_1$ = 70 Ω. The glow voltage in Fig. 15(a) was 3800 V. The voltage trace shows a 7 kV spike at the initiation of the discharge

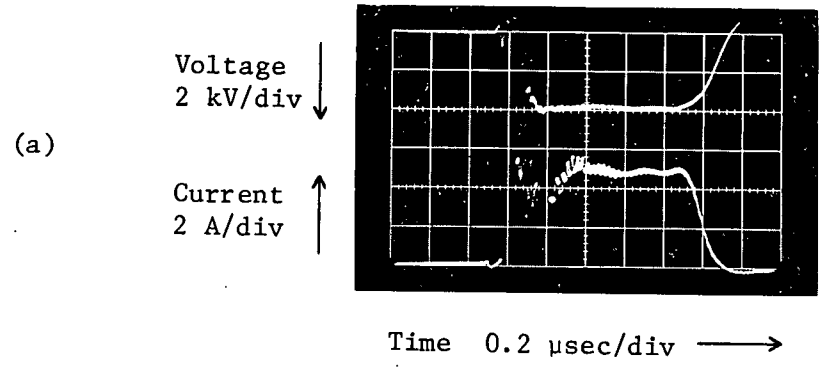


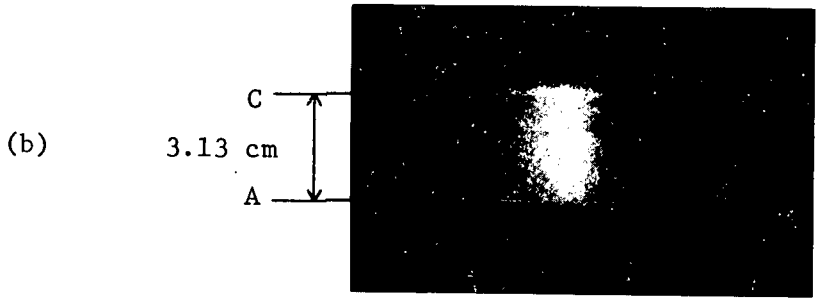


Fig. 15. (a) Voltage (upper curve) and current (lower curve) waveforms for a 94.5 He:5 Kr: 0.5 $SF_6$ mixture at 200 Torr. The discharge gap is 3.13 cm. (b) Photograph of glow discharge with a 3.13 cm gap.

due to a portion of the trigger voltage of the spark gap $SG_d$ being applied to the discharge. This coupling of the spark gap trigger voltage aided in turning on the current to the discharge. After the spark gap trigger, which lasted less than 0.1 μsec, the current in the discharge characteristically rises to a steady value, 5A in Fig. 15(a), 0.1 to 0.2 μsec after the rise of the voltage. After the current has reached a steady value it typically remains constant until an arc occurs or as long as the PFN can sustain the current, about 1 μsec in our experiments as illustrated in Fig. 15.

Figure 15(b) shows the visual appearance of the discharge illustrated in Fig. 15(a) obtained by taking 10 multiple exposures with a Polaroid camera (Type 107 film). Since the gap was 3.13 cm one has a scale from which to infer the diameter of the glow. Similar photographs were taken of discharges under conditions where no glow-to-arc transitions occurred for pressures of 100, 200, 400, 600, and 800 Torr at gaps of 0.5 cm, 1.48 cm, and 3.13 cm. For pressures of 200 Torr and above the discharge cross sectional area was independent of current and was the same as that shown in Fig. 15(b). At 100 Torr the discharge cross sectional area was about 30% larger than for the higher pressures. In general, the glow diameter showed no variation with discharge current or gap.

The variation of glow voltage with discharge gap at low currents is shown in Figs. 16 and 17 for pressures of 100 to 800 Torr and for the 5% and 15% Kr mixtures. These discharge voltages were measured for discharge currents ranging from 1 A at 800 Torr to about 4 A at 100 Torr. Over this range of current the discharge did not arc during the 1 μsec glow and the glow voltage was essentially constant. The data of Figs. 16 and 17 are consistent with a cathode fall of about 200 V for both mixtures independent of pressure at these low currents. The electric field to gas density ratio E/N in the positive column for both mixtures at the various pressures is given in Table V. The unit of E/N is the Townsend (Td) where 1 Td $\equiv 10^{-17}$ V $cm^2$.

In mixtures containing 5% Kr, E/N showed a tendency to decrease with increasing pressure whereas in the mixtures containing 15% Kr E/N was essentially independent of pressure.

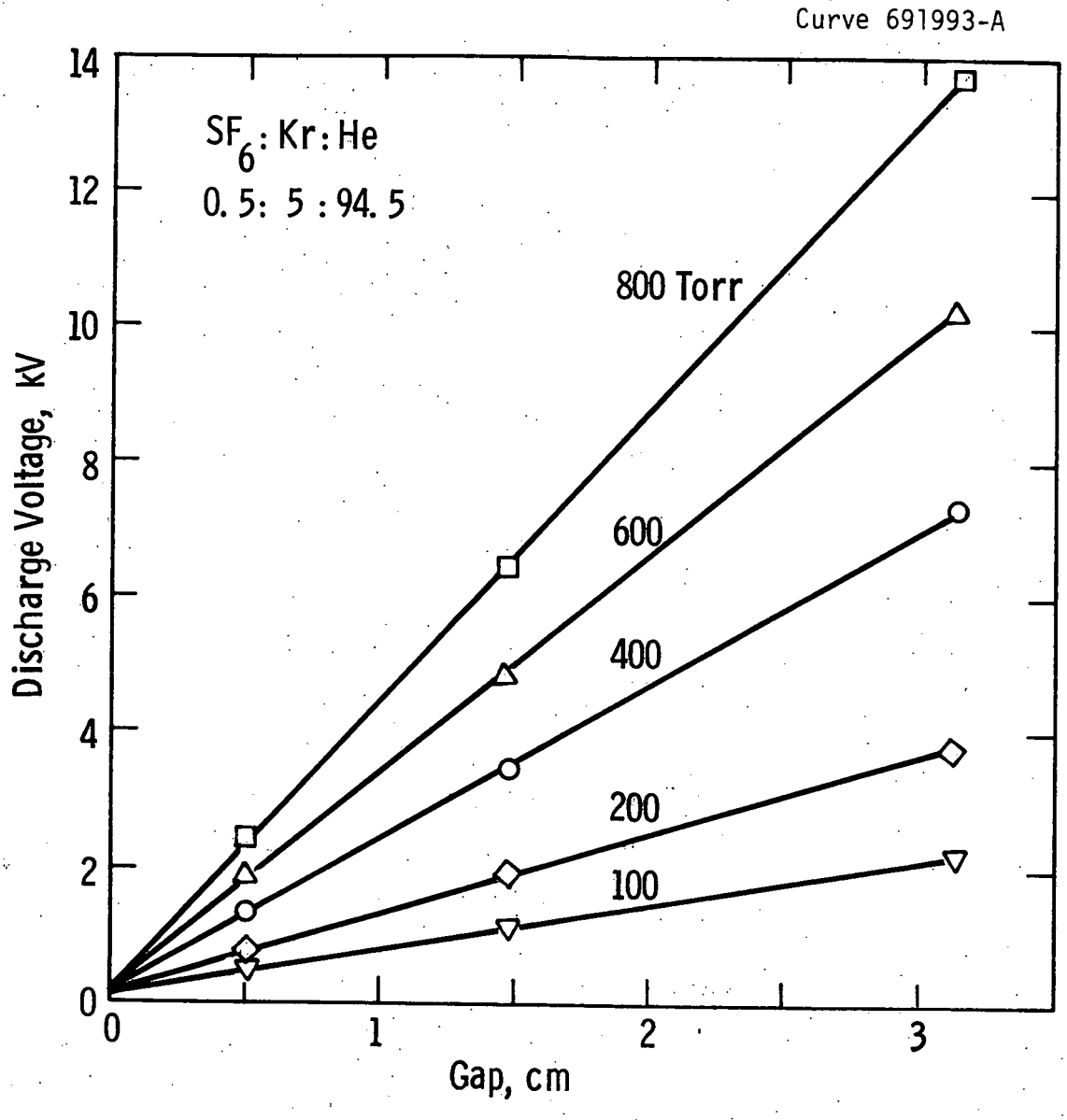


Fig. 16. Glow voltage in 5% Kr mixture as a function of pressure and gap.

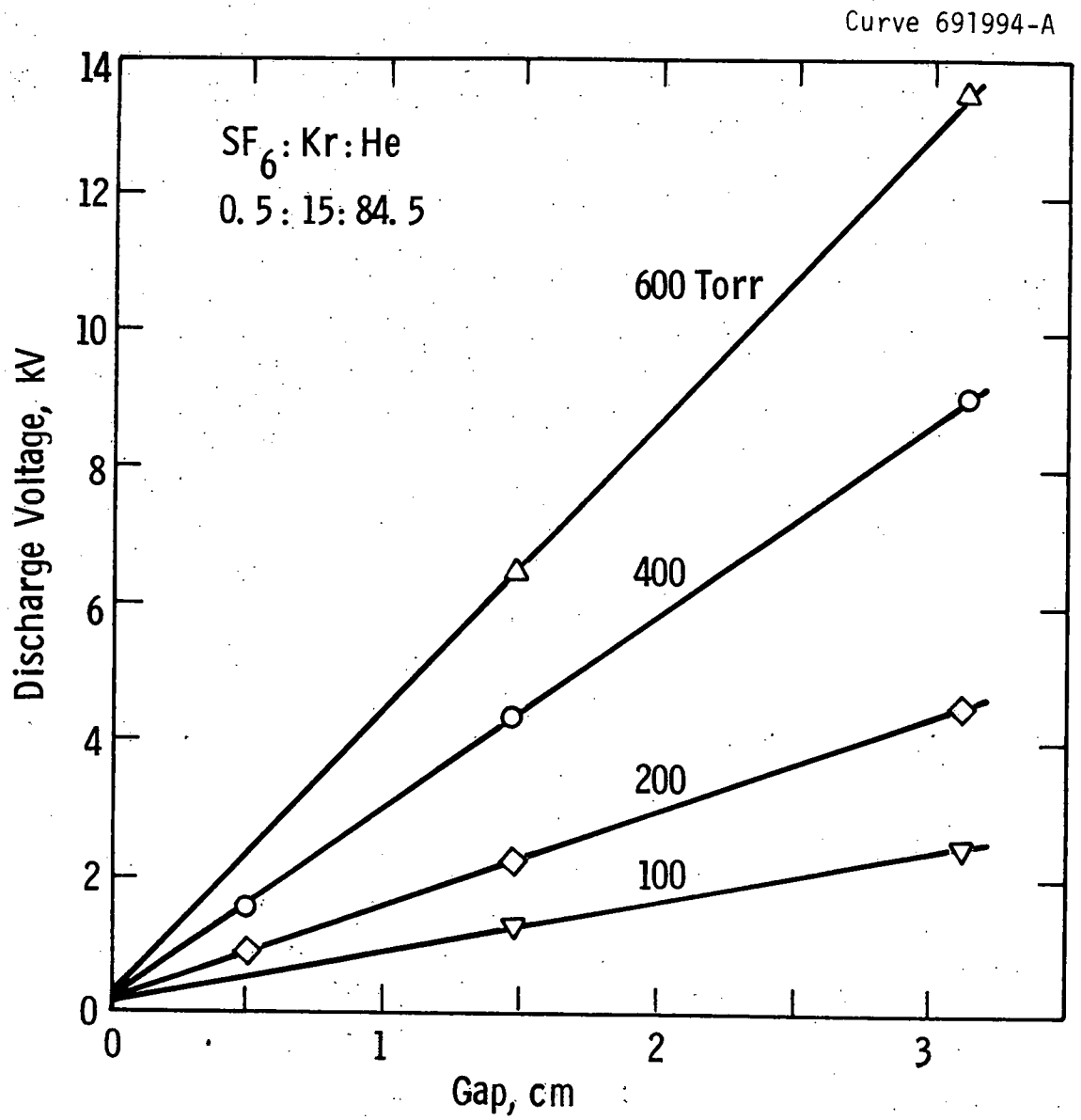


Fig. 17. Glow voltage in 15% Kr mixture as a function of pressure and gap.

Table V. E/N in positive column.

| p(Torr) | 5% Kr E/N(Td) | 15% Kr E/N(Td) |
|---|---|---|
| 100 | 19.7 | 22.2 |
| 200 | 18.2 | 21.5 |
| 400 | 17.7 | 21.8 |
| 600 | 16.6 | 21.8 |
| 800 | 16.6 | |

Measurements of glow voltage and duration of the diffuse glow phase of the discharge were made as a function of discharge current over an extended current range. Some examples of the waveforms with glow-to-arc transitions are shown in Figs. 18 and 19; here the glow-to-arc transition occurred after 0.5 μsec. As shown in the figures the glow voltage is well defined by the flatness of the voltage waveform. At pressures of 400 Torr and above the glow voltage varied by less than 3% for currents of 1 A up to a value where arcing occurred at 0.2 μsec after initiation of the glow. For $p \leq 200$ Torr, discharge currents up to 80 A were obtained and a dependence of glow voltage and cathode fall on discharge current was found. The data obtained in the 5% Kr mixture with a 0.5 cm gap are shown in Fig. 20, where the glow voltage is plotted as a function of discharge current. Data obtained at 1.48 and 3.13 cm gaps were similar; however, the glow voltage was correspondingly higher and showed less relative variation with current since the electric field in the positive column did not vary with gap.

By comparing glow voltages taken at 0.5 cm, 1.48 cm, and 3.13 cm gaps at the various currents at 200 Torr, we have determined the variation of E/N with current for currents up to about 60 A, the limit to which the discharge could be driven without arcing immediately upon initiation. The values obtained are given in Table VI for the 5% Kr mixture. The value of E/N obtained for the 15% Kr mixture at 200 Torr was 21.4 Td for currents from 2 to 50 A.

Noting that the cross sectional area of the discharge at pressures of 200 Torr and above was about 30 $cm^2$ (±20%), we can calculate an average current density. The E/N values obtained for the two mixtures as a function of average current density are shown in Fig. 21 and compared with the theoretical values discussed in Section II (Fig. 7). No 100 Torr data are included in Fig. 21 since at this pressure the discharges spread out more and the cross sectional area was about 30% greater than that at 200 Torr and above; due to curvature of the cathode the calculation of the field was relatively inaccurate. Note that the data at the left axis of Fig.21 is for $j \leq 0.1$ A/$cm^2$ and include data for j as low as 0.03 A/$cm^2$. The error bars reflect variations from shot

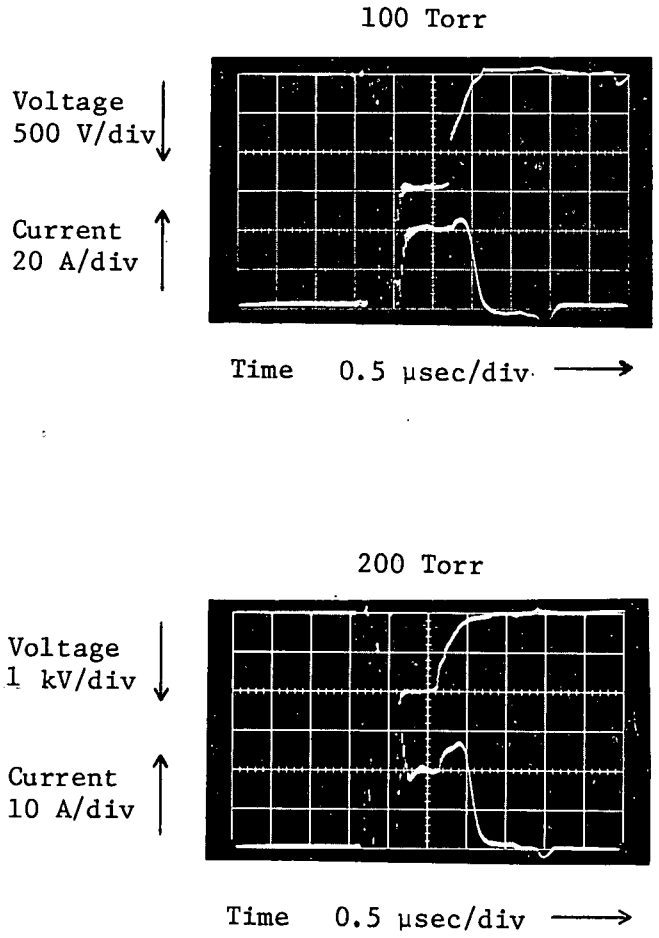


Fig. 18. Voltage and current waveforms of the glow discharge in 5% Kr mixture at 40 A in 100 Torr (upper) and at 20 A in 200 Torr, both at 1.48 cm gap.

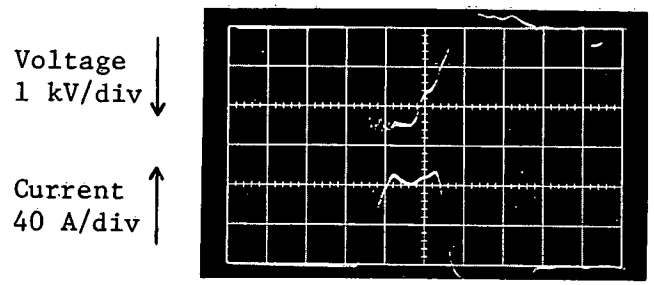


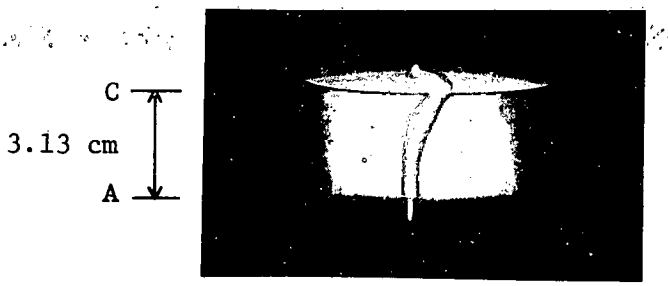


Fig. 19. Voltage and current waveforms of the glow discharge in 5% Kr mixture at 80 A in 100 Torr at 3.13 cm gap and a photograph of the diffuse glow and filamentary arc (single exposure photograph).

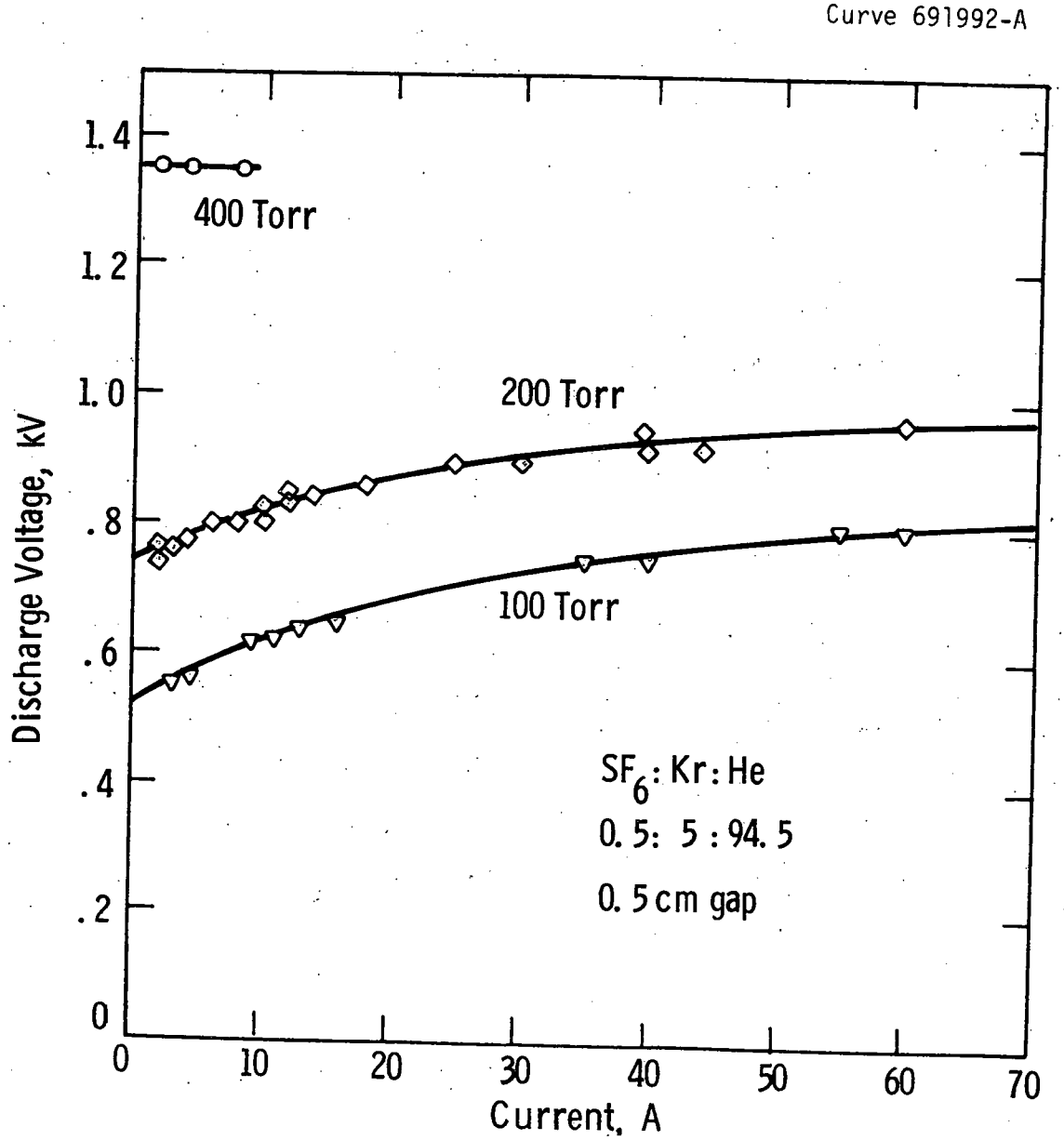


Fig. 20. Glow voltage as a function of discharge current in 5% Kr mixture at 100, 200, and 400 Torr and gap of 0.5 cm.

Table VI. E/N in the positive column at various currents in 200 Torr of 0.5%$SF_6$:5%Kr:94.5%He.

| I(A) | 2 | 10 | 20 | 30 | 50 |
|---|---|---|---|---|---|
| E/N(Td) | 17.8 | 17.5 | 17.2 | 17.1 | 16.8 |

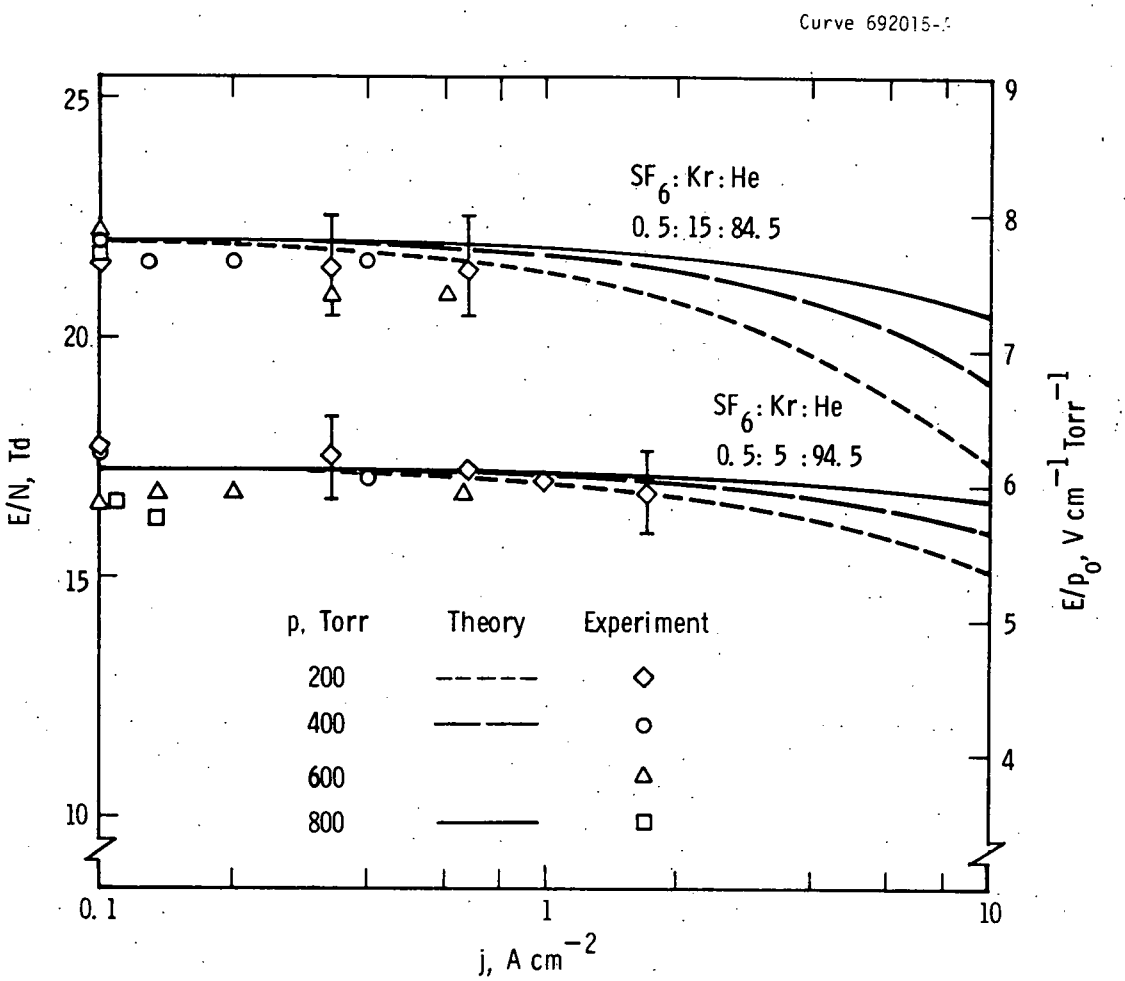


Fig. 21. E/N of the discharge as a function of average current density.

to shot, about ±3%. The over-all accuracy, including calibration uncertainties, was about 5%. The resolution of the measurements was insufficient to detect any variation with current in the 15% mixture.

Much data of the type illustrated by Figs. 18 and 19 were taken to determine the duration of the glow discharge as a function of current and pressure in both mixtures at all three gaps. Some of the measured durations are shown in Fig. 22. Although there was considerable (30 to 50%) scatter in the data, the duration appeared to vary approximately inversely with current and pressure. This is indicated by the (arbitrary) straight lines in Fig. 22. The failure of the lines to go through the origin of Fig. 22 suggests an error in determining the correct starting time for the steady state on the waveforms of the type shown in Figs. 18 and 19. Glows in the 15% mixtures had durations approximately 1/3 as long as those in the 5% mixtures at the same total pressures and currents. Although not shown in Fig. 22, 1 μsec glows were obtained in the 15% mixtures at values of $(pI)^{-1}$ corresponding to an extrapolation of the data. This data is consistent with an energy density limit of the glow discharge before arcing.

The growth rate of the observed instability can be estimated from the recorded waveforms, where the transition to an arc is shown as a collapse of the voltage, accompanied by a slight increase in the current. (The circuit ballasting prevented the total discharge current from increasing significantly with the formation of an arc.) The time for the voltage collapse from the steady-state value was primarily a function of gap spacing, increasing with increasing gap spacing. For example, in both mixtures at a pressure of 200 Torr the glow-to-arc transition occurred in times of approximately 50 nsec at a gap of 0.5 cm, increasing to about 300 nsec at a gap of 3.13 cm. These times were representative of both mixtures at all pressures examined. The glow-to-arc transition time did, however, decrease somewhat with increasing current in the glow. The times for voltage collapse and the dependence on gap spacing is consistent with a time for propagation of a filament across the gap. Since the current was prevented from increasing by the external circuit impedance, the development of a filament must occur by

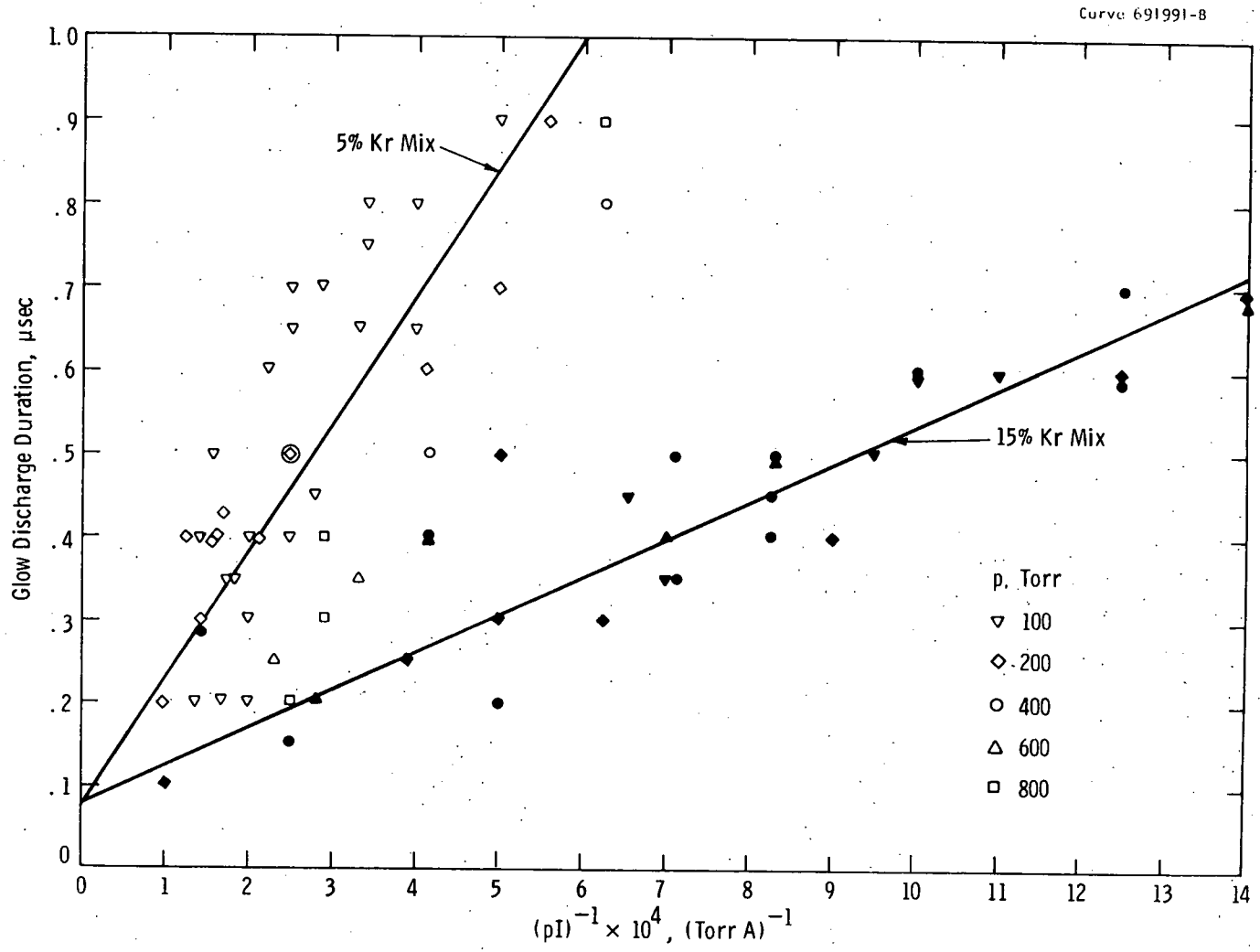


Fig. 22. Glow discharge duration as a function of $(pI)^{-1}$.

current constriction; the glow extinguishes over the discharge volume as the filament extends between both electrodes. Photographs of partially developed filamentary structures indicated that the filaments originated on the anode screen.

We have evaluated the time constant for growth of the instability analyzed in Ref. 38. The characteristic growth time is given by Eq. (27) for the case of self-sustained discharges in $SF_6$:Kr:He mixtures. In this case the variables a and b which appear in Eq. (27) are evaluated using Eqs. (31) and (32), respectively. We have evaluated the instability growth time, $\tau$, over the pressure range $200 \leq p \leq 800$ Torr for both of the $SF_6$:Kr:He mixtures which were studied experimentally. The results are shown in Fig. 23. The calculated values of $\tau$ are strongly decreasing functions of current density. $\tau$ also decreases with increasing pressure. However, the sensitivity of $\tau$ to pressure varies with current density.

The calculated growth times are such that if this instability were occurring, it would have been observed. That is, the discharge electrical characteristics after discharge initiation would have been found to change with time rather than remain constant until the observed termination of the steady-state glow by the more rapid process. The measured instability growth time at glow termination was found to depend only weakly on current, pressure, and mixture, in contrast with the calculated variation. Rather, the measured growth time depended most strongly on gap spacing. There is no such dependence in the calculated characteristic time of Fig. 23. Thus, there is no apparent similarity between the instability of Ref. 38 and that observed in the experiments reported here.

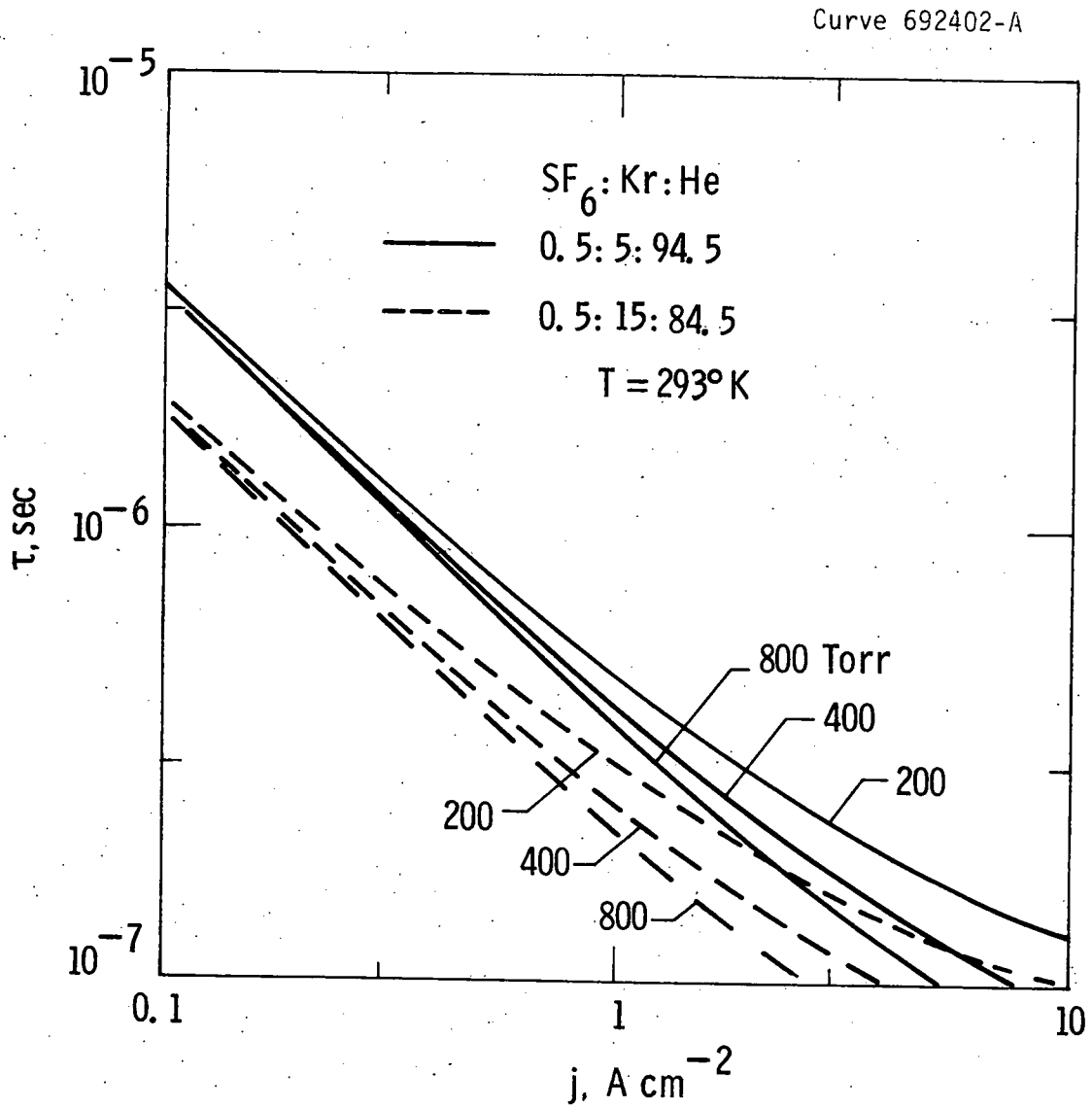


Fig. 23. Calculated time constants for instability growth predicted by Eq. (27) vs. current density.

## IV. SUMMARY AND CONCLUSIONS

This report describes a combined experimental and theoretical study of the maintenance and stability of diffuse glow discharges in attaching gas mixtures involving processes similar to those in laser discharges. Steady-state, self-sustained, diffuse glow discharges have been established experimentally in attachment-controlled $SF_6$:Kr:He gas mixtures similar to those utilized in short-pulse excimer laser discharges. The gas mixtures contained 0.5% $SF_6$ and 5% to 15% Kr, with total pressures of 100-800 Torr and current densities up to about 2 $A/cm^2$.

A theoretical model has been developed to describe electrical characteristics of the discharges. The model includes electron-impact ionization by single-step and two-step processes, the latter involving krypton metastables. For the experimental conditions, attachment to $SF_6$ is shown to be the dominant electron loss process. The model yields electric field-current density relationships for the positive column.

An experimental system has been designed and constructed for generating uv-preionized, self-sustained discharges, with facilities for electrical and optical measurements. The positive column electric fields were determined by measuring steady-state discharge voltages at different anode-cathode gap spacings. Current densities were determined from total current measurements and discharge cross-sectional areas obtained photographically. Measured and calculated electrical characteristics are in good agreement. This indicates an understanding of the primary glow discharge processes.

Termination of the glow by glow-to-arc instabilities has been observed. Glow durations have been measured, as have the times for arcs to develop after the onset of the glow-to-arc transition. The latter appear to be consistent with times for propagation of filaments between the electrodes. The propagation velocities suggested by these measurements appear to be consistent with measured velocities in spark discharge studies.

Discharge operation is not limited by the instability analyzed by Daugherty, Mangano, and Jacob.[38] The observed discharges violate the stability criterion that results from their analysis, which apparently describes a bulk effect corresponding to a negative V-I characteristic. This effect is stabilized with appropriate circuit ballasting; it does not represent a fundamental limitation to operation of self-sustained discharges in attaching gases, as their analysis might imply.

The results of the present study indicate that the primary limitation to steady discharge operation is the glow-to-arc transition involving current redistribution and filament formation within the diffuse glow. The details of the filament formation have not been explored in this study. However, this work provides a data base of discharge operating characteristics to serve as a foundation for a more detailed examination of the growth of this important instability.

## V. REFERENCES


1. G. L. Rogoff, Phys. Fluids 15, 1931-1940 (1972).

2. S. C. Haydon, in A Survey of Phenomena in Ionized Gases: Invited Papers, Eighth Int. Conf. on Phenomena in Ionized Gases, Vienna, 1967, (International Atomic Energy Agency, Vienna, 1968), p. 495.

3. L. J. Denes, Westinghouse R&D Center (private communication). These observations were made with a uv-initiated, near-atmospheric pressure, $CO_2$:$N_2$:He laser discharge in a near-uniform-field gap. For a description of a similar type of laser discharge, see L. J. Denes and L. A. Weaver, J. Appl. Phys. 44, 4125 (1973).

4. J. L. Pack, Westinghouse R&D Center (private communication).

5. See, for example, J. D. Daugherty, in Principles of Laser Plasmas (Wiley, N.Y., 1976), G. Bekefi, Ed., p. 369.

6. See, for example, A. A. Doran, Z. Physik 208, 427-440 (1968); M. C. Cavenor and J. Meyer, Aust. J. Phys. 22, 155-167 (1969); I. D. Chalmers, H. Duffy, and D. J. Tedford, Proc. R. Soc. Lond. A 329, 171-191 (1972).

7. K. G. Emeleus, Conf. on Negative Ions, Univ. of Liverpool, March 1971, Paper 10.

8. G. L. Rogoff, Bull. Am. Phys. Soc. 19, 147 (1974).

9. G. L. Rogoff, Bull. Am. Phys. Soc. 20, 234 (1975).

10. A. J. Andrews, A. J. Kearsley, C. E. Webb, and S. C. Haydon, Opt. Commun. 20, 265-268 (1977); V. N. Ischenko, V. N. Lisitsyn, and A. M. Razhev, Appl. Phys. 12, 55-58 (1977) and Opt. Commun. 21, 30-32 (1977).

11. L. S. Frost and A. V. Phelps, Phys. Rev. 127, 1621-1633 (1962).

12. P. Luft, "Description of a Backward Prolongation Program for Computing Transport Coefficients", JILA Information Center Report No. 14 (Joint Institute for Laboratory Astrophysics, Boulder, 1975).

13. J. J. Lowke, A. V. Phelps, and B. W. Irwin, J. Appl. Phys. 44, 4664-4671 (1973).

14. J. H. Jacob and J. A. Mangano, Appl. Phys. Lett. 28, 724-726 (1976).

15. L. S. Frost and A. V. Phelps, Phys. Rev. 136, A1538-A1545 (1964).

16. D. Rapp and P. Englander-Golden, J. Chem. Phys. 43, 1464-1479 (1965).

17. M. Schaper and H. Scheibner, Beit. Plasma Physik 9, 45-57 (1969).

18. S. E. Kuprianov, Opt. Spect. 20, 85-86 (1966).

19. A. A. Kruithof, Physica 7, 519-540 (1940).

20. J. H. Jacob and J. A. Mangano, Appl. Phys. Lett. 29, 467-469 (1976).

21. S. K. Srivastava, S. Trajmar, A. Chutjian, and W. Williams, J. Chem. Phys. 64, 2767-2771 (1976).

22. C. L. Chen and P. J. Chantry, private communication.

23. L. G. Christophorou, D. L. McCorkle, and J. G. Carter, J. Chem. Phys. 54, 253-260 (1971).

24. B. Lehman, Z. Naturforsch. 25a, 1755-1757 (1970).

25. M. S. Bhalla and J. D. Craggs, Proc. Phys. Soc. 80, 151-160 (1962).

26. H. A. Boyd and G. C. Crichton, Proc. I.E.E. 118, 1872-1877 (1971).

27. T. H. Teich and B. Sangi, "Proc. Int'l. Symposium on High Voltage Technology, Munich, 1972" (Verband Deutscher Elektrotechniker, Munich, 1972) pp. 391-395.

28. V. N. Maller and M. S. Naidu, Proc. I.E.E. 123, 107-108 (1976).

29. M. S. Naidu and A. N. Prasad, J. Phys. D 5, 1090-1095 (1972).

30. W. H. Long, Jr., Appl. Phys. Lett. 31, 391-394 (1977).

31. W. H. Long, Jr. (private communication).

32. O. P. Judd (private communication).

33. J. N. Bardsley and M. A. Biondi, in Advances in Atomic and Molecular Physics 6 (Academic Press, New York, 1970).

34. This recombination process has been mentioned in several papers, e.g., a) C. A. Brau and J. J. Ewing, Appl. Phys. Lett. 27, 435-437 (1975); b) R. C. Sze and R. P. Scott, J. Appl. Phys. 47, 5492 (1976); c) V. N. Ishchenko, V. N. Lisitsyn, and A. M. Razhev, Appl. Phys. 12, 55 (1977); d) J. Hsia, Appl. Phys. Lett. 30, 101 (1977), however, no quantitative data appear to be available for $Kr^+$-$SF_6^-$. The number used is typical of gases for which data exist.

35. J. E. Velazco, J. H. Kolts, and D. W. Setser, J. Chem. Phys. 65, 3468-3480 (1976).

36. E. Nasser, Fundamentals of Gaseous Ionization and Plasma Electronics (Wiley, New York, 1971), p. 163.

37. P. L. Patterson, J. Chem. Phys. 53, 696-704 (1970).

38. J. D. Daugherty, J. A. Mangano, and J. H. Jacob, Appl. Phys. Lett. 28, 581-583 (1976).

39. J. D. Daugherty, in Principles of Laser Plasmas (Wiley, N.Y., 1976), G. Bekefi, Ed., pp. 405-406.

40. See, for example, J. F. Waymouth, Electrical Discharge Lamps (MIT Press, Cambridge, Mass., 1971), pp. 27, 28, 118.